Neotectonic and Paleoseismic Onshore-Offshore integrated study of the Carboneras Fault (Eastern Betics, SE Iberia)

Estudio integrado tierra-mar de la Neotectonica y Paleosismología de la Falla de Carboneras (Béticas Orientales, SE Península Ibérica)

Ximena Moreno Mota

RISKNAT
Departament de Geodinàmica i Geofísica
Universitat de Barcelona

Barcelona Center for Subsurface Imaging
Unidad de tecnología Marina
Consejo Superior de Investigaciones Científicas

Neotectonic and Paleoseismic Onshore-Offshore integrated study of the Carboneras Fault (Eastern Betics, SE Iberia)

Estudio integrado tierra-mar de la Neotectonica y Paleosismología de la Falla de Carboneras (Béticas Orientales, SE Península Ibérica)

Memoria presentada por

Ximena Moreno Mota

para optar al grado de Doctora en Geología

Esta memoria se ha realizado dentro del programa de Ciències de la Terra (bienio 2005-2006) de la Universitat de Barcelona bajo la dirección de las Doctoras Eulàlia Masana Closa y Eulàlia Gràcia Mont

Barcelona, Julio de 2010

Part I: Introduction

Chapter 1: Approach and objectives

1.1. Interest of the study: Paleoseismology of slow structures

Paleoseismology is concerned with large prehistoric earthquakes in order to extend the seismic catalogue back in time. This is especially important in slow slip-rate regions hosting large earthquakes with long return periods ($<10^3$ years), regions where the historical catalogues are shorter than recurrence intervals (Santanach and Masana, 2001). In addition, the location of historical epicenters is often too inaccurate to precisely establish a relationship with specific faults. Uncertainty largely increases when the epicenter is located offshore. Preparedness in the face of future earthquakes entails the detection and the characterization of all the possible seismogenic sources in the region, including those that may not have ruptured in the historical period. A number of initiatives have therefore been developed: Early Warning Systems (e.g. Indian Ocean), long term monitoring of seismic activity (GPS and broad-band OBS), and active fault databases for a global understanding of the earth (GEM project: www.globalquakemodel.org) and more local seismic hazard modelling such as the SHARE project for Europe: www.share-eu.org, and Iberfault project for the Iberian Peninsula: www.iberfault.org.

Major plate boundaries are mainly located under oceans and inland seas with the results that most of the large earthquakes are marine events triggered by submarine fault systems. Innovations on offshore geophysical techniques and dating methods during the last decades have made considerable headway in the analysis of submerged structures. Despite the limitation of the fault not being directly accessible for observing, sampling and measuring at its intersection with the Earth surface, working in the sub-aqueous environment has a number of advantages, i.e. good spatial coverage, continuous sedimentation throughout a long temporal span, minimized erosion, and very limited human modification. Consequently, it is possible to image extensive areas through geophysical techniques (Pantosti and Gràcia, 2010). Nevertheless, the accuracy required for paleoseismic studies is rarely achieved and very high-resolution techniques are needed. Moreover, onshore and offshore fields are usually not merged, obliging us to limit the structure at the shoreline. This lack of land-to-sea connection can lead to a serious underestimation of the fault parameters (geometry, number of segments, etc.) with grave implications for seismic hazard modelling. In fact, the opportunity of working onshore and offshore along the same structure allows us to make full use of each environment, direct fault observations onshore and the continuous sedimentation offshore.

In the Southeastern Iberian Margin, the compression between the African and Eurasian Plates is characterized by a moderate seismicity and a slow NW-SE convergence (4-5 mm/yr) (Argus et al., 1989; DeMets et al., 1990). In southeastern Spain, this shortening is mainly absorbed by a left-lateral strike-slip fault system known as the Eastern Betics Shear Zone (EBSZ). Several historical events have also occurred along this system, characterized by a shallow low-to-moderate magnitude instrumental seismicity and a clear surface expression. However, its seismogenic potential continuous to be poorly understood (Masana et al., 2005). The very long recurrence period of the Alhama de Murcia fault, the only fault proven so far to be seismogenic in the system (Martínez-Díaz et al., 2003; Masana et al., 2004), suggests the presence of other seismogenic faults that may have remained silent within the historical period, or may not have been correctly attributed to any historical earthquake. This area of the Iberian Peninsula is nowadays a densely populated area dedicated to tourism and agriculture. Moreover, a gas pipeline from Algeria feeding Southern Europe crosses the Alboran Sea and the Almería province overlaying potentially active faults such as the Carboneras Fault. In this highly vulnerable framework, a large magnitude earthquake poses a serious threat to the region.

This work seeks to characterize the most recent tectonic activity of the seismically silent but morphologically expressive Carboneras Fault, the longest and southernmost fault of the EBSZ, embracing both onshore and offshore portions of the fault. To this end, a multidisciplinary and multiscale study is carried out. The results will contribute realistic paleoseismic values of the Carboneras Fault to the national active fault database (García-Mayordomo et al., 2010a). The availability of an updated active fault database is crucial for obtaining realistic seismogenic source models (García-Mayordomo et al., 2010b), and for better assessing the seismic hazard risk of the region.

1.2. Objectives

1.2.1. Main objectives

The main objectives of this thesis are:

1) To characterize the neotectonic evolution of the Carboneras Fault through an integrated and multidisciplinary geological and geophysical approach along and around the fault zone.

2) To determine the past seismic activity of the Carboneras Fault by adopting a paleoseismic approach in order to establish its seismic parameters: geometry, slip-rates, recurrence interval, elapsed time since the last earthquake and maximum magnitude earthquake.

Moreover, the characterization of the fault parameters will allow the evaluation the seismic potential of this structure, and will contribute to the seismic catalogue and fault databases, which is essential for a better seismic hazard modelling and assessment.

1.2.2. Specific Objectives

Onshore and offshore studies were carried out in parallel. Specific onshore objectives consisted in:

-A regional geological and geomorphological analysis of the complete fault trace and the deposits involved in the deformation complemented by localised geophysical studies was performed to 1) understand its geometry and structural geology, 2) establish its short and long-term neotectonic activity, and 3) detect the most suitable sites for more detailed paleoseismic analysis.

-A detailed paleoseismic study was centred on selected sites along the fault trace and based on detailed geomorphic mapping, microtopographic levelling, high-resolution geophysical prospecting, trenching and dating. These analyses allow the determination of the seismogenic nature of the fault and its seismic parameters through the identification of past earthquakes in the geological record and the constraining of their chronology.

Specific offshore objectives consisted in:

-An analysis of the geomorphology and seismostratigraphy of the Almería Margin in order to observe the architecture of the Carboneras Fault at depth and

the tectono-sedimentary evolution throughout the Neogene. To this end, a multidisciplinary and multiscale approach was adopted using multibeam bathymetry mapping and a dense grid of seismic profiles with different degrees of vertical resolution.

-A paleoseismic analysis through geomorphic and stratigraphic observations in order to obtain the fault parameters offshore. The highest resolution methods such as high resolution bathymetry and very-high resolution seismics were used.

The final objective of this work is to merge the onshore and offshore results in order to integrate, compare and complement the information obtained in both parts of the fault. This integration provides a “big picture” of the Carboneras Fault and characterizes its entire extension making a realistic contribution to seismic hazard analysis.

1.3. Terminology

The terminology used in earthquake geology can vary depending on the specific interest and on the area of study. The main concepts and the definitions of the most common terms in this thesis and the uses given to them in this thesis in case of ambiguity are listed below.

Neotectonics is the study of motions and deformations of the Earth's crust during the current tectonic regime or neotectonic period (Pavlides and Mountrakis, 1986; Pavlides, 1989). The **neotectonic period** is considered as the youngest, unfinished tectonic stage. In the study area, the neotectonic period started in the Late Miocene (Bousquet and Montenat, 1974; García-Dueñas et al., 1984; Sanz de Galdeano, 1988; Viseras et al., 2004) and coincides with the last compressional phase of the Alpine orogeny when the tectonic movements are related to the convergence between the African and Iberian Peninsula. According to this definition, a neotectonic fault is a fault with evidence of tectonic activity during the neotectonic period.

Active Tectonics is the ongoing deformation of the earth's surface. It also defined as the tectonic movements that are expected to occur within a future time span and are of concern to society (Wallace, 1986). The social interest in forecasting tectonic activity entails steps to mitigate the seismic hazards, i.e. special attention on rates, styles, and patterns of deformation, within a period of several decades to several hundred years, the duration for which we plan the lifetime of buildings and important facilities such as dams and power plants (Keller and Pinter, 1996). However, in order to predict tectonic events over this period, we must study these processes over a much longer time scale because earthquakes caused by particular faults may have long return periods (10^3-10^6 years).

An **active fault** is widely defined as a fault that is currently moving (Wallace, 1981; Wallace, 1986), but this is an ambiguous definition as it is strongly dependent on the location and interest of the study. To get round this ambiguity, earthquake geologists usually specify the time concerning the activity of the fault. For instance, in areas of high recurrence events such as California, an active fault will be considered as the one that has moved along the Holocene, whereas in slower tectonic regimes, an active fault scientist will consider longer periods (e.g. throughout the Quaternary or even since the Pliocene). A more accurate description is achieved when considering the active fault as the fault that has been active during the current tectonic regime and is currently moving or is capable of producing a seismic event. In this study, an active fault is a fault with evidence of tectonic movement during the Quaternary, the latest stage of the neotectonic period and the time span of concern to society.

A **capable fault** is a term used in nuclear power plants and nuclear storage regulations (U.S.Nuclear-Regulatory-Comission, 2007), and it is defined as a tectonic structure that can generate both vibratory ground motion and tectonic surface deformation such as faulting or folding at or near the earth's surface in the present seismotectonic regime. It has at least one of the following characteristics:

1) Presence of surface or near-surface deformation of landforms or geological deposits of a recurring nature within the last approximately 500,000 years or at least once in the last approximately 50,000 years.

2) A reasonable association with one or more moderate to large earthquakes or sustained earthquake activity, usually accompanied by significant surface deformation.

3) A structural association with a capable tectonic source that has characteristics of either item (1) or (2) (above) so that movement in one could be reasonably expected to be accompanied by movement in the other.

Paleoseismology is the study of the identification and evaluation of prehistoric earthquakes (Sieh, 1978; Wallace, 1986), especially their location, timing, and size, through the interpretation of geological evidence produced during individual paleoearthquakes. Paleoseismology differs from other fields of earthquake geology because it concerns the almost instantaneous deformation of landforms and sediments during individual earthquakes. Paleoseismology is concerned with records of large (Mw>6.5) earthquakes because small and moderate-sized earthquakes rarely generate geological evidence preserved near the surface (McCalpin, 2009).

Paleoearthquakes are prehistoric earthquakes (Sieh, 1978; Wallace, 1986), i.e. earthquakes that occurred before the time of written accounts with some quantitative observations of earthquakes (McCalpin, 2009). In the southeastern Iberian Peninsula, written records of historical earthquakes start with the Muslim period of *Al-Andalus* in the early VIII century and became more frequent with the Christian conquest of the *Reino de Granada* in 1487 (Espinar-Moreno, 1994; Martínez-Solarez, 1995). For this reason, in the study area, a paleoearthquake is an earthquake that occurred before the VIII century.

The term **characteristic earthquake** was adopted by Schwartz and Coppersmith (1984) to simplify the analysis of paleoseismicity for a region where seismogenic faults breaks periodically producing similar deformation events, i.e. with a similar slip and similar seismic energy release.

An **Event horizon** is interpreted as the ground surface at the time of a paleoearthquake (Pantosti et al., 1993). An event horizon is stratigraphically defined by either scarp-derived colluvium that buries the pre-faulting surface, and/or by unconformities that develop as a result of warping and subsequent deposition (McCalpin, 2009). By dating the deposits below and above we can constrain the age of the earthquake event.

A **Colluvial Wedge** is a chaotic and wedge-shaped colluvial deposit formed at the base of a fault scarp as a consequence of the degradation of this unstable topography. Colluvial wedges are interpreted as having formed soon after the surface-rupturing event overlying the pre-faulting surface. Thus, the base of colluvial wedges are considered as event horizons (Schwartz and Coppersmith, 1984).

Paleoseismic Parameters are the fault parameters used in seismic risk analysis. They describe the characteristics of the fault and its behaviour, such as the **fault geometry** (orientation, length, fault depth and width, number and geometry of segments), **slip-rate** (average amount of movement per time, measured in mm/a), **displacement per event** (the characteristic slip in a single earthquake), **recurrence interval** (the time between an earthquake and the previous one), **elapsed time** (time passed since the last earthquake), in this manuscript considered until 2010, and **maximum magnitude** (the largest earthquake magnitude that a seismic source is capable of generating under the current tectonic regime). Although these parameters may differ from earthquake to earthquake, they are calculated as average parameters in order to give an idea of the activity of the fault.

Empirical Relationships: Some of the paleoseismic parameters are used to estimate a probable paleoearthquake magnitude by comparing this with the data of rupture length and slip of known magnitude earthquakes. The length of surface rupture and the maximum displacement along continental fault traces are by far the most commonly used parameters. Wells and Coppersmith (1994) compared worldwide databases with paleoseismic parameters, obtaining global empirical relationships for different types of rupture mechanisms. Stirling et al. (2002) updated and extended the Wells and Coppersmith (1994) database to analyse separately the pre-instrumental and instrumental period earthquakes, but do not differentiate between rupture mechanisms. Stirling et al. (2002) observed a significant difference between the relationship of large earthquakes (Mw > 6) and moderate events (Mw = 4-6). Some authors propose that these relationships vary significantly between seismotectonic regions (i. e. Pavlides and Caputo, 2004; Dowrick and Rhoades, 2004), and specific regional regression analyses are built when possible. Other studies suggest that relationships are strongly dependent on the rupture mechanisms but not on the tectonic setting (Vakov, 1996). In any case,

no relationship can be obtain for slow slip regions such as the Southern Iberian Peninsula, and then, only the global relationship (Wells and Coppersmith, 1994; Stirling et al., 2002) can be used to obtain an approximation, always assuming an associated inherent error.

The **Magnitude of an earthquake** is a number that characterizes the relative size of an earthquake. The magnitude is typically based on the measurement of the maximum motion recorded by a seismograph. Some of the scales defined are local or Richter magnitude (ML), surface-wave magnitude (Ms), body-wave magnitude (mb for short period, mB for long period), and moment magnitude (Mw). **Moment magnitude** is the most recent scale. It differs from the others because it is not based on measured seismogram peaks but is related to the seismic moment (M_0) of an earthquake (Kanamori, 1977; Hanks and Kanamori, 1979). The seismic moment measures the size of the earthquake considering the fault rupture area, the average slip, and the strain necessary to overcome the friction force. It is measured from seismograms using very long-period waves. Moment magnitude is nowadays used worldwide for moderate and large earthquakes because (1) it can be easily calculated with modern instruments, (2) it is directly link to physical parameters such as fault area, fault slip, and energy, (3) it can be independently estimated by geodetic, field-geological and by seismographic methods, and (4) it is the only magnitude scale that adequately estimates the size of the source of very large earthquakes (Yeats et al., 1997).

1.4. Paleoseismology: background

The early studies of paleoearthquakes in the late XIX century were limited to descriptions of the surface rupture zone with special emphasis on fault scarps. Almost a century later, the new plate tectonics theory and the occurrence of successive large earthquakes prompted researchers to carry out studies with a paleoseismological content in countries with scientific infrastructures where tectonic activity was high: United States, Japan, Russia and New Zealand. Clarence Allen and Robert Wallace carried out studies on the San Andreas fault (Allen, 1968; Wallace, 1970), establishing the basis of this new discipline called paleoseismology. It was Clark et al (1972) who first published a paleoseismic study using the trenching technique, and in subsequent years Kerry Sieh considerably improved this technique (Sieh, 1978; Sieh and Jahns, 1984) by composite logging, 3D trenching and especially by applying dating techniques to constrain the ages of paleoearthquakes. Interest in paleoseismology has notably increased since the 1970s (Ran and Deng, 1999), and new techniques are constantly being developed, improving the accuracy of the results and allowing exploration of new environments such as the water-covered earth surface.

The reliance on paleoseismic data is necessary to understand the fault behaviour in places where the historical and instrumental records of large earthquakes are short and incomplete. Paleoseismology focuses on the almost instantaneous deformation of landforms and sediments during earthquakes with the aim of analysing the distribution of individual paleoearthquakes in space and time. For this reason, paleoseismologists look for seismic evidence produced by earthquakes large enough to distort stratigraphic units, displaced landforms, or generate earthquake-induced sedimentation.

McCalpin (2009) classified paleoseismic evidence into three hierarchical levels based on genesis, location, and timing (Table 1.1). At the highest level, paleoseismic evidence is distinguished as primary or secondary. Primary paleoseismic evidence is produced by tectonic deformation resulting from coseismic slip along a fault plane. Secondary paleoseismic evidence is produced by earthquake shaking, or by erosional and depositional responses to shaking and coseismic elevation changes. At the second level, paleoseismic features are further distinguished as being on or above a fault trace (on-fault or near-field features), or removed from or far above a fault trace (off-fault or far-field features). The third level distinguishes instantaneous features formed at the time of the earthquake (coseismic) from delayed response (postseismic) features formed by geological processes after coseismic deformation and seismic shaking cease. Paleoseismic evidence is preserved as either landforms (geomorphological evidence) or as deposits and structures (stratigraphic evidence), and this distinction often determines our approach to paleoseismic field investigations. The geomorphological approach commonly involves deducing the amount of fault displacement during paleoearthquakes from the measurements of landform deformation. The stratigraphic approach focuses on

deducing fault displacement and earthquake recurrence from measurement and dating of deformed strata in exposures.

Table 1.1: Classification of paleoseismic evidence (from McCalpin, 2009)

Primary evidence (produced by tectonic deformation)			
On-fault		**Off-fault**	
Coseismic	**Postseismic**	**Coseismic**	**Postseismic**
Geomorphological expression: -Fault scarps -Fissures -Folds -Moletracks -Pressure ridges	*Geomorphological expression:* -Afterslip contribution to on-fault coseismic features -Colluvial aprons	*Geomorphological expression:* -Tilted surfaces -Uplifted shorelines -Subsided shorelines	*Geomorphological expression:* -Tectonic alluvial terraces -Afterslip contributions to off-fault coseismic features
Stratigraphic expression: -Faulted strata -Folded strata -Unconformities -Disconformities	*Stratigraphic expression:* -Scarp-derived colluvial wedges -Fissure fills	*Stratigraphic expression:* -Tsunami deposits and erosional unconformities caused by tsunamis	*Stratigraphic expression:* -Erosional unconformities and deposits induced by uplift, subsidence, and tilting
Secondary evidence (produced by seismic shaking)			
On-fault		**Off-fault**	
Coseismic	**Postseismic**	**Coseismic**	**Postseismic**
Geomorphic expression: -Sand blows -Landslides and lateral spreads in the fault zone -Disturbed trees and tree-throw craters	*Geomorphic expression:* -Retrogressive landslides originating in the fault zone	*Geomorphic expression:* -Sand blows -Landslides and lateral spreads beyond the fault zone - Disturbed trees and tree-throw craters - Fissures and Sackungen - Subsidence from sediment compaction	*Geomorphic expression:* -Retrogressive landslides beyond the fault zone
Stratigraphic expression: -Sand dikes and sills -Soft-sediment deformation -Landslide toe thrust	*Stratigraphic expression:* -Sediments deposited from retrogressive landslides	*Stratigraphic expression:* -Sand dikes -Filled craters -Soft-sediment deformation structures -Turbidites	*Stratigraphic expression:* -Erosion or deposition in response to retrogressive landslides or surface features such as fissures, lateral spreads, or sand blows, or other forms of landscape disturbance

Typically, the stratigraphic analysis by trenches is one of the most fruitful areas of paleoseismic studies and provides descriptions of stratigraphic evidence that are widely discussed and commonly accepted. In stratigraphic exposures, paleoearthquakes are typically recognized in section from six general types of evidence: (1) upward termination of fault displacement against a unconformity (Fig. 1.1a,d), (2) abrupt changes in vertical separation of strata as faults are traced upsection or downsection, (3) abrupt changes in thickness of strata or facies across a fault, (4) fissures and sand blows in the stratigraphic sequence (Fig. 1.1b,f), (5) angular unconformities produced by folding and tilting, and (6) colluvial wedges shed from small scarps (Fig. 1.1e)

(McCalpin, 2009). Moreover, soft-sediment deformation structures or liquefactions are also interpreted as secondary off-fault coseismic indicators of seismic activity (Fig.1.1c).

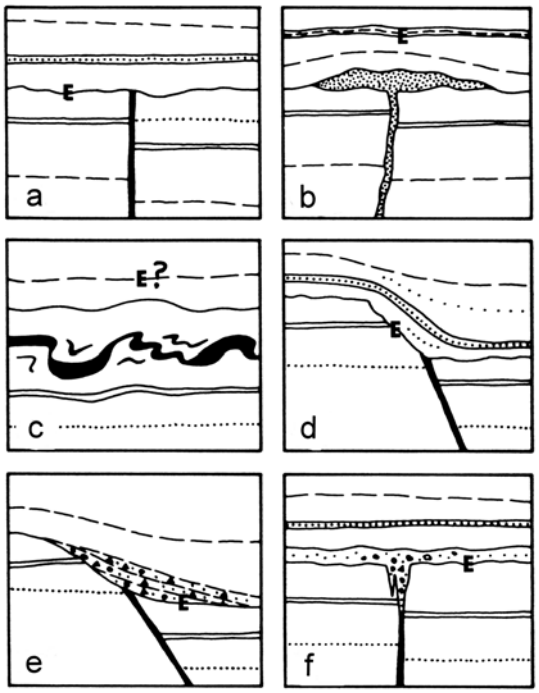

Figure 1.1. Schematic diagrams of typical stratigraphic indicators of paleoearthquakes in strike-slip environments. In all examples strata have been offset by a single event, either along faults (thick black lines) or sand dikes (stippled pattern) (from Allen, 1986).

Selecting a good site for stratigraphic observation is critical because the production and preservation of paleoseismic evidence can change along the fault with the result that cross sections can vary dramatically depending on the site. It is necessary for paleoseismologists to understand the geomorphological settings in order to accurately interpret a stratigraphic cross section and to avoid as possible paleoseismic underrepresentations. In the schematic figure 1.2 a few idealized succession of stratigraphic evidences (colluvial wedges, flower structures, blinded faults, sand blows and craters) are shown in hypothetical cross sections along a strike-slip fault with fault stepovers between segments (map of the fault in the centre).

Like other scientific disciplines, paleoseismology suffers from a series of limitations. The most notable limitation is that the geological record of paleoearthquakes is usually incomplete. This is because (1) many earthquakes are too small to produce observable primary or secondary evidence, (2) special conditions are needed to provide stratigraphic or geomorphological paleoseismic evidence, and (3) paleoseismic evidence can be quickly modified, obscured, or removed by common superficial processes (McCalpin, 2009). In many cases, the preservation of paleoseismic evidence is determined by the relative rates of erosion and deposition versus deformation (e.g. Wallace, 1986). In addition, deformation during large recent earthquakes may obscure evidence of smaller, older earthquakes. And disruption of strata by biological agents (such as roots or rodolites) or low sedimentation rates may

also obscure paleoseismic evidence. Given that biological agents act only during low sedimentation rate periods, highly bioturbated units represent long hiatuses in deposition, during which event horizons may be obliterated or superimposed (Yeats et al., 1997). When paleoseismic features are not preserved (or not observed), seismic history will be underrepresented (Sieh, 1981), i.e. the paleoseismologist underestimates the number of paleoearthquakes of a given magnitude at a site.

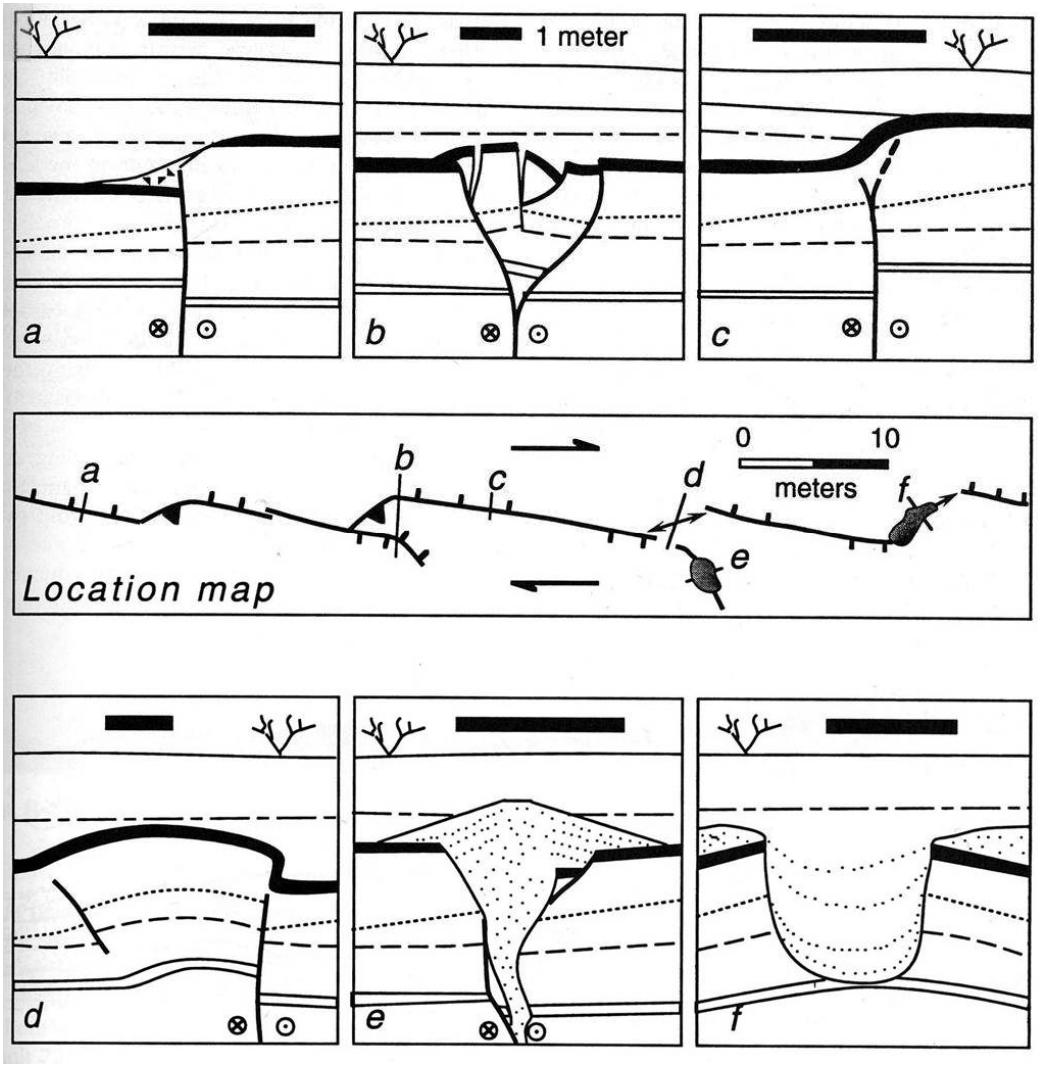

Figure 1.2. Idealized cross sections across a strike-slip fault showing variation of evidence of paleo-earthquake along the fault trace. The top of the solid black bed is the event horizon. Shaded horizontal bars are 1 meter long. Lines with arrows on location map indicate crests of anticlinal folds. Mismatches of strata across some of the faults is an indication of strike-slip motion (from Yeats et al., 1997).

1.5. Strike-slip faults and active strike-slip faults

Strike-slip faults occur in several plate-tectonic environments: linking ridges, trenches, in obliquely-convergent plate margins and in crust extension settings. Strike-slip faults are often the longest faults on continental landmasses and typically have a pronounced geomorphological expression, as in the case of the Carboneras Fault, one of the longest structures of the southeastern Iberian Peninsula. Many highly densely populated regions are located close to or directly on strike-slip faults (e.g. California, Marmara Sea, Japan or New Zealand). The social impact caused by great historical earthquakes (e.g. the San Francisco earthquake in 1906) has focused attention on strike-slip faults in paleoseismic studies.

Strike-slip ruptures commonly begin with en-échelon fault and fold segments (Wilcox et al., 1973). Right-lateral faults generate left-stepping fractures, and left-lateral faults right-stepping fractures (Yeats et al., 1997). The mechanics and evolution of these faults were analysed in laboratory experiments by Riedel (1929) and Tchalenko (1970), using clay-cake experiments. The first structures to be formed were termed *Riedel* or *R-shears* by Tchalenko, and for a left-lateral strike they are formed at a counter-clockwise angle of about 12º to the shear, following the Coulomb criterion (Yeats et al., 1997). As shearing continues, the Riedel structures increase in length and new en-échelon Riedel shears are developed at lower angles. And as more slip occurs, more Riedel shears are produced with an even smaller angular deviation, also producing *P shears*, shears parallel to the total relative movement, forming small clockwise angles. When the slip is large enough, integration of Riedel and P shears occurs to form continuous *principal displacement shears*, and nearly all slip occurs in these shears. In other words, as the displacement increases, fault segments start to link. Areas between linked segments may define alternating areas of localized convergence and divergence (Cunningham and Mann, 2007). Thus, we may define restraining bends as those that accommodate local contraction (transpression), and releasing bends as those that accommodate extension (transtension). Restraining and releasing bends are widespread, forming major mountain ranges (topographic uplift) and rift basins (subsidence areas), but can also be found forming small-scale features (Mann, 2007). Elongated basins (e.g. sag ponds) are formed because of extension in domains of releasing bends, and pull-apart basins evolve between overstepping strike-slip faults (Sylvester, 1988).

As shown in figure 1.3, there is a wide range of tectonic features associated with strike-slip faulting. On a left-lateral fault, releasing double bends (such as a bend to the left and then to the right) or stepovers to the left tend to create transtensional features such as normal faults, monoclinal folds, and rhomboidal grabens. Bends and stepovers of opposite symmetry induce transpressive structures such as pressure ridges, thrust faults, and folds (McCalpin, 2009). Double restraining and releasing bends commonly define positive and negative flower-structures, respectively, or duplexes in plan view

(Woodcock and Fischer, 1986). Single bends commonly have horsetail splay fault geometries in plan view, with strike-slip displacements terminally accommodated by oblique-slip and dip-slip faulting (McClay and Bonora, 2001).

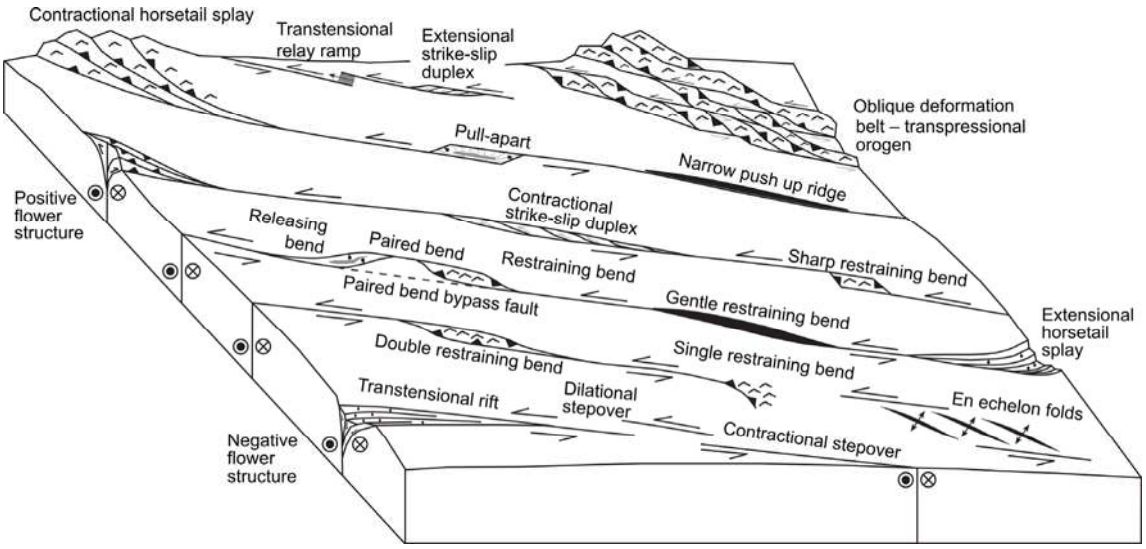

Figure 1.3. Tectonic features associated with strike-slip restraining and releasing bends (from Cunningham and Mann, 2007).

The main strike-slip fault plane is typically sub-vertical, with a dip variation within ca. 10°, and the fault strike is parallel to the regional shear direction. Near the main fault plane, subsidiary fault planes may branch upward from the main fault, forming flower-structure morphologies but may also converge again up-dip into a single fault strand, which is rare in other tectonic environments. Individual faults in a strike-slip zone are more undulatory in section than normal or reverse faults, and may change dip often in the space of several decimetres to meters (McCalpin, 2009). Active strike-slip faults frequently show fault creep, which may be steady or episodic, pre-seismic, co-seismic, or post-seismic, depending on the constitutive properties and the nature of the static strain field among a number of other factors (Sylvester, 1988).

Active strike-slip faulting produces a characteristic assemblage of landforms (Fig. 1.4) including linear valleys, offset or deflected streams, shutter ridges, sag ponds, pressure ridges, benches, scarps, and small horsts and grabens (Keller, 1986). Strike-slip faults also transport non-tectonic landforms laterally while the erosional and depositional processes forming them continue to operate. This lateral transport causes the most obvious geomorphic effects when faults strike perpendicular to the direction of stream transport. Three landforms are typically used to reconstruct paleoseismic offset histories: fluvial terraces, stream channels, and alluvial fans. Two conditions are essential for an ideal paleoseismic site: the slip must be localized in a narrow fault zone

and small geomorphological features such as gullies crossing the fault zone must be frequently formed (McCalpin, 2009).

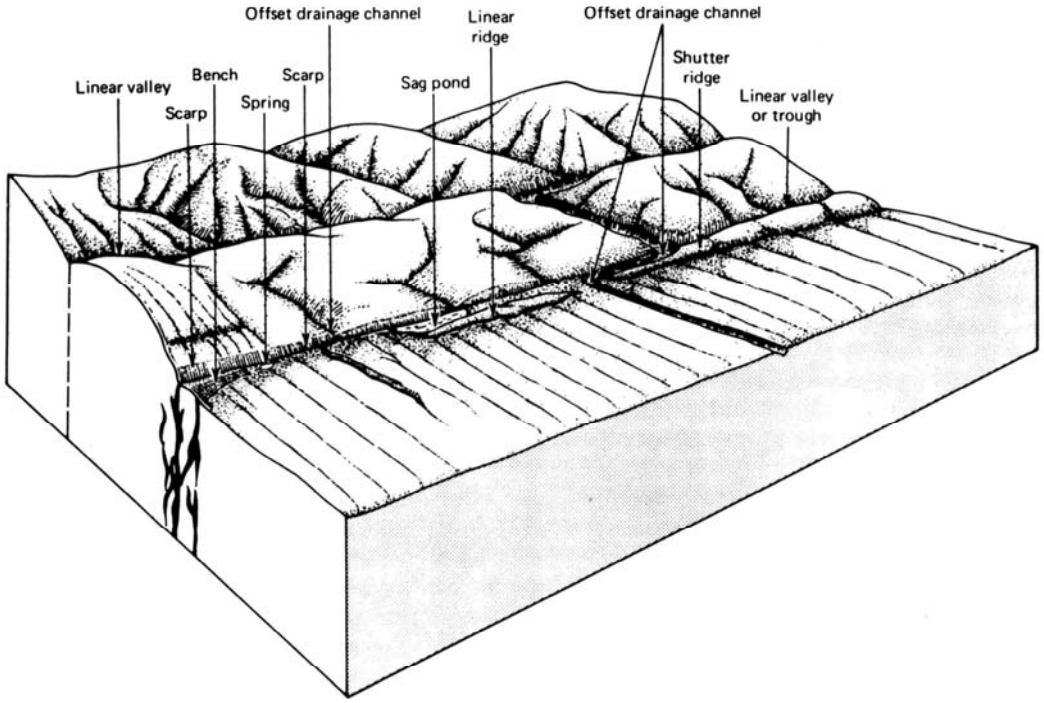

Figure 1.4. Block diagram of landforms associated with strike-slip faulting (from Costa and Baker, 1981).

Chapter 2: Geological Setting

2.1. Tectonic framework

The South Iberian Peninsula hosts the slow convergent plate boundary between Africa and Eurasia at rates of 4.5-5.6 mm/yr (Argus et al., 1989; DeMets et al., 1990; McClusky et al., 2003). This boundary is characterized by a 400 km wide active deformation zone distributed among a series of structures (e.g. Sartori et al., 1994) (Fig 2.1 and 2.2). This complex collisional plate boundary is formed by an arcuate Alpine orogen (Fig. 2.1) whose geodynamic mechanisms are still not well understood (Fontbote and Vera, 1986; Sanz de Galdeano, 1997). The Alboran basin located in the middle of the orogen is bounded by the Straits of Gibraltar to the west, by the Betic Cordillera (SE Spain) to the north and by the Rif-Tell Ranges (NW Africa) to the south (Fig 2.2), forming the Gibraltar Arc. The orogen extends smoothly westwards to the Gulf of Cadiz and eastwards to the Balearic Islands, constraining the northern part of the Algero-Balear basin.

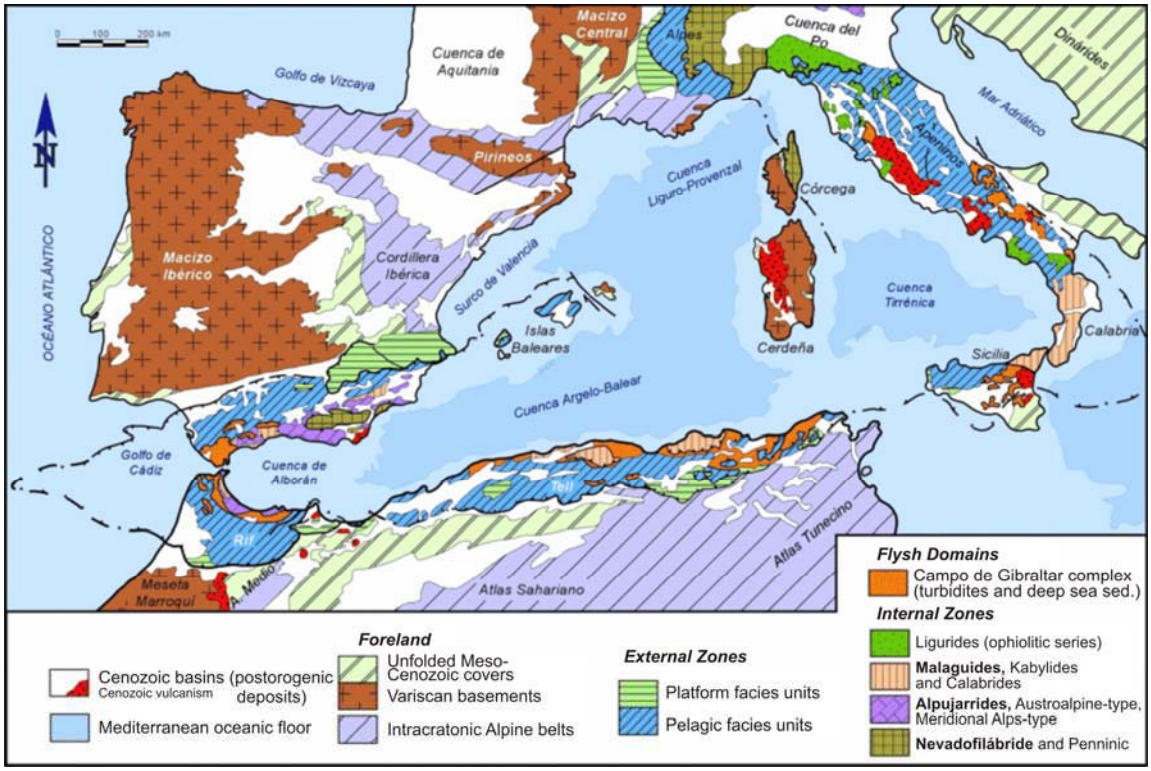

Figure 2.1. Geological map of the westernmost segment of the Alpine Peri-Mediterranean Orogen (modified from Vera, 2004).

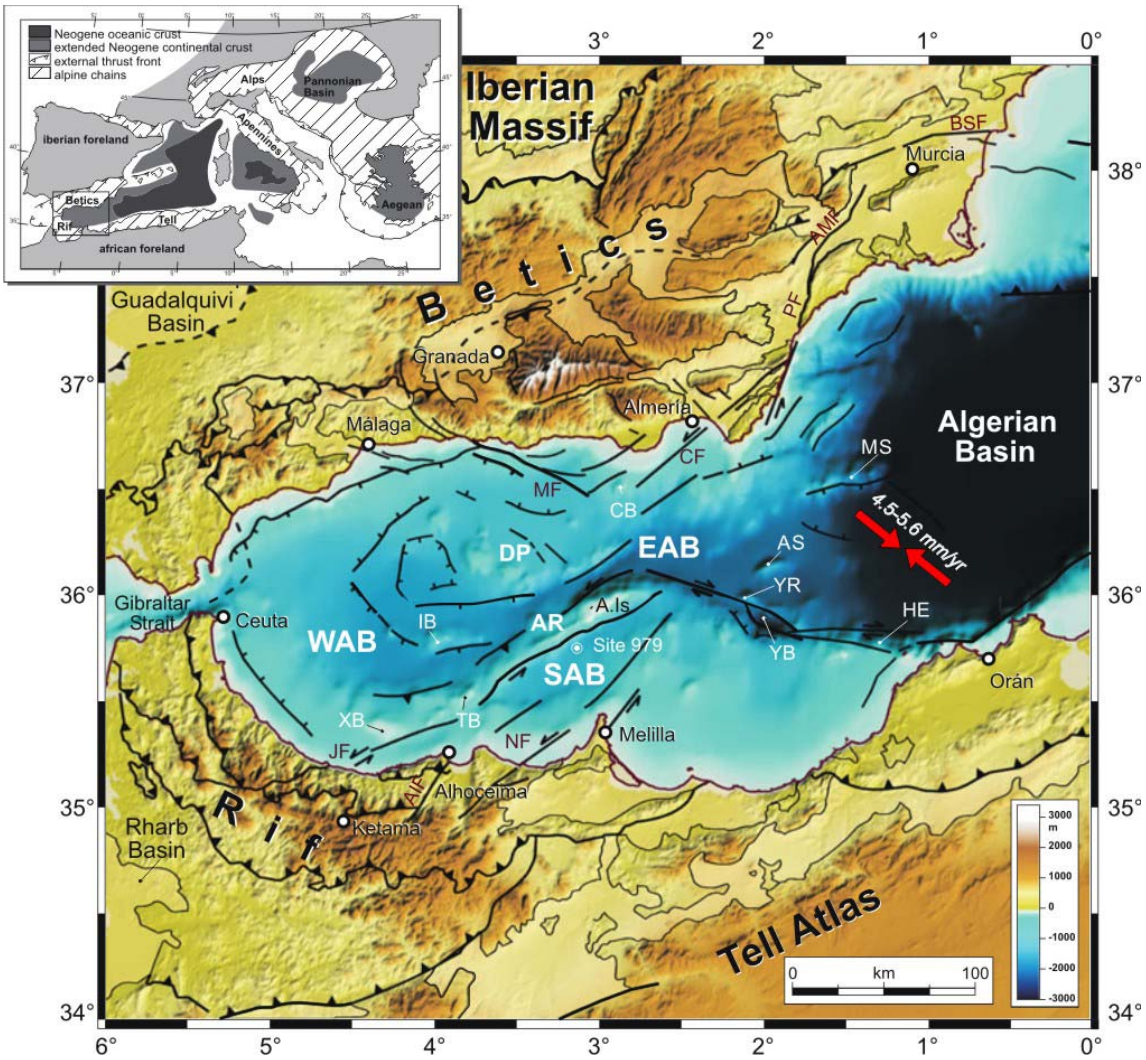

Figure 2.2. Topography of the Gibraltar Arc and major tectonic features of the Alboran Sea (simplified from Comas et al. 1999) (digital topography extracted from the SRTM (USGS-NASA) global database, combined with GEBCO 97 (IOC-IHO) for the offshore region). Inset tectonic sketch of the Mediterranean Sea, showing the Neogene extensional basins and the fronts of the surrounding Alpine thrust belts (from Comas et al. 1999). A. Is. Alboran Island, AR Alboran Ridge, AS Al-Mansour Seamount, CB Chella Bank, CF Carboneras Fault, DP Djibouti Plateau, EAB East Alboran Basin, HE Habibas Escarpment, IB Ibn-Batouta Bank, JF Jebha Fault, AI Al-Idrissi Fault, MF Maro-Nerja Fault, MS Maimonides Seamount, NF Nekor Fault, PF Palomares Fault, AMF Alhama de Murcia Fault, BSF Bajo Segura Fault, SAB South Alboran Basin, TB Tofiño Bank, XB Xauen Bank, YB Yusuf Basin, YR Yusuf Ridge, WAB West Alboran Basin (modified from Martínez-García et al., 2010).

The Betic Cordillera is traditionally divided into three main geological units: a) the External Zones (or Alboran domain) in the north hosting Mesozoic to Tertiary original Iberian paleomargin rocks, b) the Internal (or Betic) Zones in the south hosting foreign units, and c) the *Campo de Gibraltar* Complex located locally in between and formed by sedimentary cover removed from its original substratum and unaffected by

alpine metamorphism (Vera and Martín-Algarra, 2004). The Internal Zones, where the study area is located, consists mainly of a thrust stack of Triassic and older clastic metasedimentary rocks (Weijermars, 1991) and corresponds to the most deformed and metamorphosed units of the orogen. The overthrust occurred before the Late Eocene (Paquet, 1969) by an antiform pile formed up-down by the *Maláguide*, *Alpujárride* and *Nevadofilábride* nappe complexes (Vera and Martín-Algarra, 2004). Owing to its relative location, the *Malaguide* rocks show a lower level of metamorphism whereas marbles indicating higher phases of metamophism become more frequent in lower units through the *Alpujárride* and *Nevadofilábride* nappes. The thrust contacts between these major complexes were reactivated during the fragmentation process as low-angle normal faults under regional extensional tectonics (Galindo Zaldívar et al., 1989; Aldaya et al., 1991; García-Dueñas et al., 1992; Jabaloy et al., 1993). After several compressional and extensional episodes (Bousquet, 1979), the neotectonic period (the last 9 Ma) commenced (Bousquet and Montenat, 1974; García-Dueñas et al., 1984; Sanz de Galdeano, 1988; Viseras et al., 2004) and a compressional stress field with a N-S to NW-SE shortening direction was established (Bousquet et al., 1976; Martínez-Díaz et al., 2001). New structures were formed and previous structures were reactivated by the changes in the stress direction of shortening (Bousquet and Montenat, 1974). Discordantly on the metamorphic basement, Miocene to Quaternary deposits fill the post-orogenic intramontane basins, due to the neotectonic activity of the major fault zones and folds deforming the previous structures (Weijermars, 1991). Neogene calc-alkaline and alkaline volcanic complexes crop out in the Cabo de Gata volcanic region and extend into the Alboran Sea, forming volcanic seamounts, such as the Chella Bank (Fernández-Soler, 1996; Duggen et al., 2004). This volcanism was formed as a result of extensional processes attributed to the development of the Alboran Basin after the Alpine collision (Platt and Vissers, 1989; Fernández-Soler, 2001). The volcanic deposits are intercalated with and overlain by Neogene sedimentary rocks (Martín et al., 2003).

2.2. The Eastern Betic Shear Zone

In the southeast of the Iberian Peninsula, the shortening between Eurasian and African plates is accommodated by the NE-SW trending left-lateral strike-slip (Fig. 2.3) known as the Eastern Betics Shear Zone (EBSZ) (Bousquet, 1979; Sanz de Galdeano, 1990). This shear zone is located in the Internal Zones of the Betic Cordillera, and consists of the following main faults, from north to south: Bajo Segura Fault, Carrascoy Fault, Alhama de Murcia Fault, Palomares Fault and Carboneras Fault (Fig 2.3). Together with its extension to the southwest under the Alboran Sea (Fig. 2.2) (Bousquet et al., 1975), it has been termed the Trans Alboran Shear Zone (TASZ) (Frizon de Lamotte et al., 1980; De Larouzière et al., 1988), which is probably linked to the north-African NE-SW faults (Martínez-Díaz and Hernández-Enrile, 2004).

The Bajo Segura Fault (BSF) extends from the north-eastern tip of the Carrascoy Range with an ENE-WSW orientation, changing rapidly to a more E-W orientation eastwards towards the coast for more than 25 km, from where it continues offshore (Fig. 2.3a,b). This structure limits the Vega Baja del Segura Holocene depression to the south. The BSF is a reverse and blind fault that is expressed in the surface as an E-W antiform, the Bajo Segura anticline. It is the only fault from the EBSZ trending E-W and with a reverse kinematics. The Carrascoy Fault (CaF), is 33 km long and trends NE-SW, bounding the NW part of the Carrascoy Range (Fig. 2.3a). This fault runs parallel to the Alhama de Murcia Fault (AMF) for about 20 km, on the other side of the Guadalentín depression, about 9 km to the SE. The Alhama de Murcia fault bounds the Neogene Guadalentín depression to the NW and trends NE-SW (Fig. 2.3a). It is, together with the Carboneras Fault Zone (CFZ), one of the longest structures of the EBSZ. The northern part of the Palomares Fault (PF) runs more or less parallel to the southern termination of the AMF, with a NE-SW orientation, for about 30 km but 12 km to the east, at the opposite boundary of the Guadalentín depression (Fig. 2.3a). Then, it changes its orientation to NNE-SSW for at least 30 km onshore. North of the Carboneras Village, the PF intersects the CFZ at the shoreline. This intersection and the offshore continuation of the PF are poorly documented. At the southern tip of the EBSZ, the Carboneras Fault Zone, strikes N050-N065º. It is located onshore in the province of Almería, and extends for 50 km from the mouth of the Alías River to the north, passing the Salinas de Cabo de Gata shoreline towards the SW. From there it extends offshore to the south along the shelf and the Alboran Sea for 90 km (Fig. 2.3a).

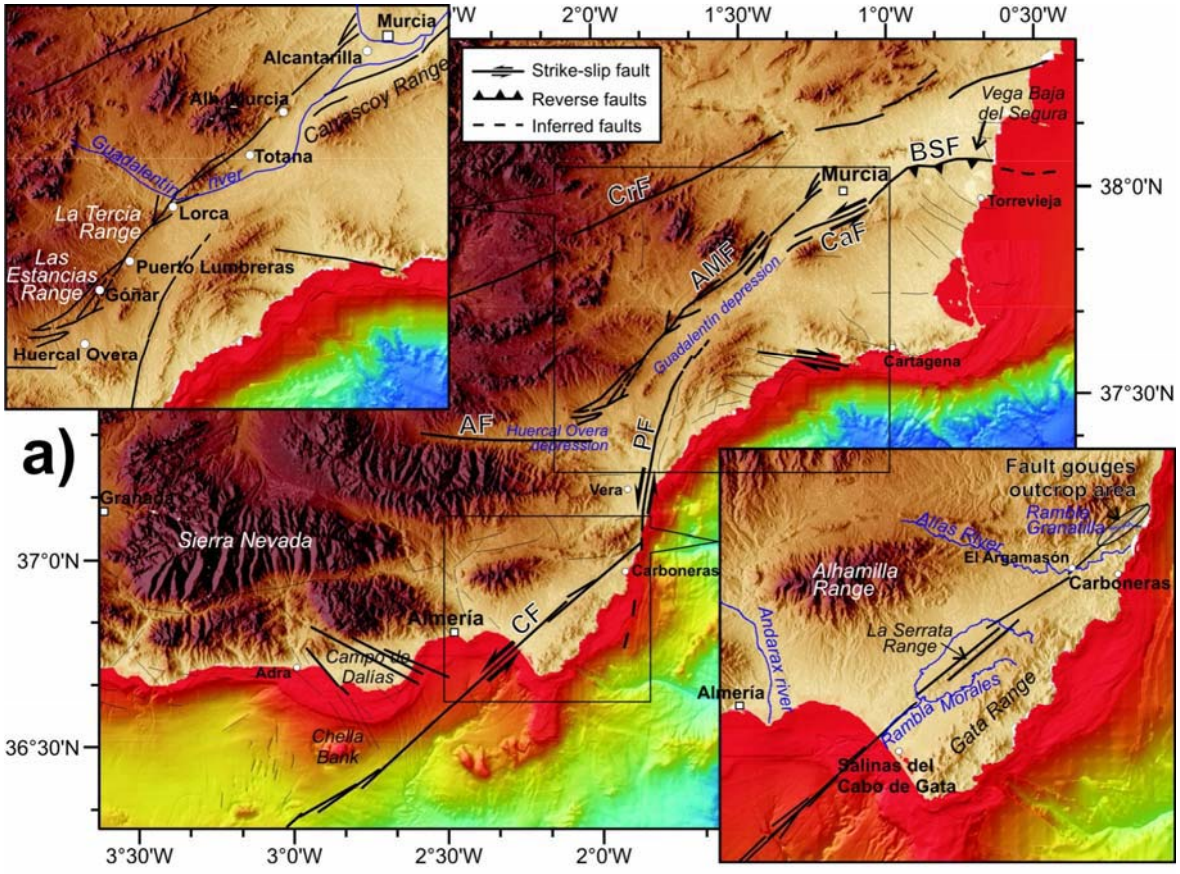
a)
Murcia
Alcantarilla
Alb. Murcia
Totana
Guadalentín river
Carrascoy Range
La Tercia Range
Lorca
Las Estancias Range
Puerto Lumbreras
Gónar
Huercal Overa
Strike-slip fault
Reverse faults
Inferred faults
Vega Baja del Segura
BSF
Torrevieja
CrF
AMF
CaF
Guadalentín depression
Cartagena
AF
Huercal Overa depression
PF
Vera
Granada
Sierra Nevada
Carboneras
Almería
CF
Campo de Dalías
Adra
Chella Bank
Fault gouges outcrop area
Rambla Granatilla
Alías River
El Argamasón
Alhamilla Range
La Serrata Range
Andarax river
Rambla Morales
Gata Range
Salinas del Cabo de Gata
2°0'W
1°30'W
1°0'W
0°30'W
38°0'N
37°30'N
37°0'N
36°30'N
3°30'W
3°0'W
2°30'W
2°0'W

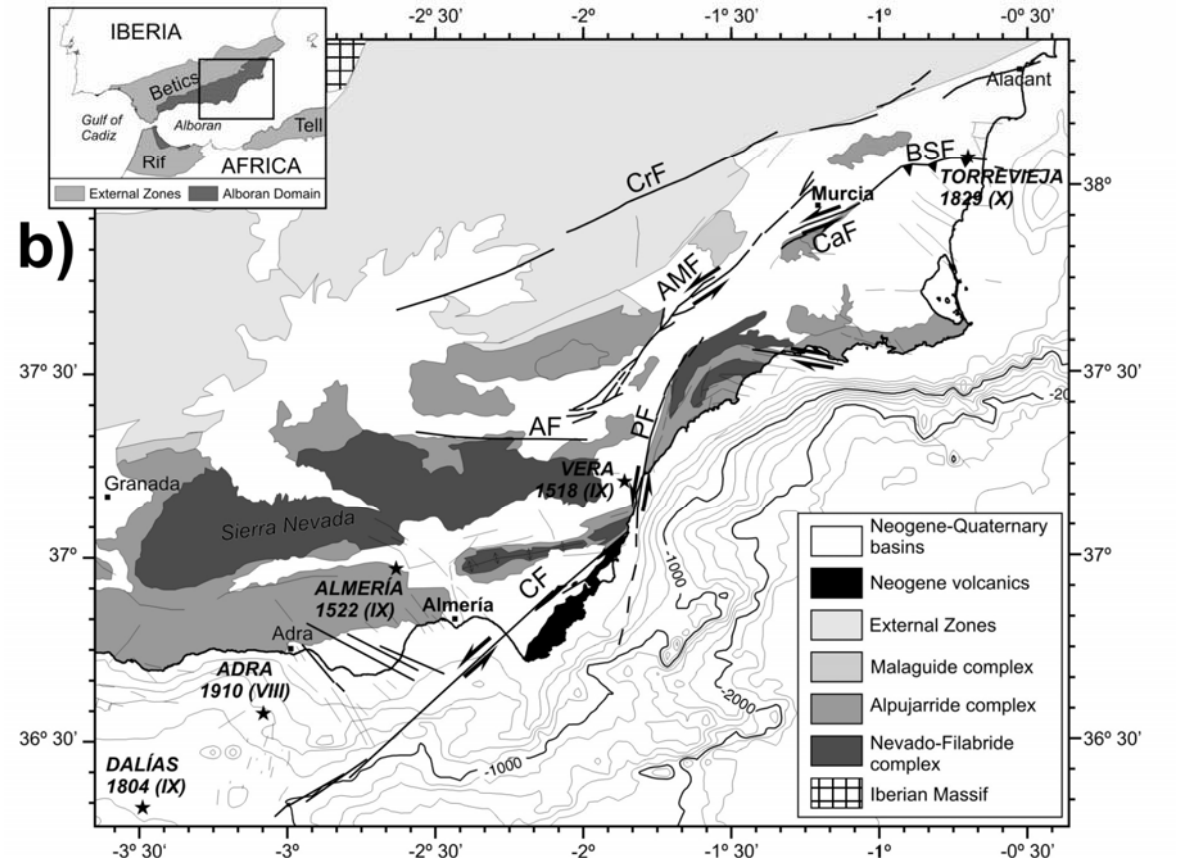
b)
IBERIA
Betics
Gulf of Cadiz
Alboran
Tell
Rif
AFRICA
External Zones
Alboran Domain
-2° 30'
-2°
-1° 30'
-1°
-0° 30'
Alacant
CrF
BSF
TORREVIEJA 1829 (X)
Murcia
CaF
AMF
38°
37° 30'
AF
PF
VERA 1518 (IX)
Granada
Sierra Nevada
37°
ALMERÍA 1522 (IX)
Almería
CF
Adra
ADRA 1910 (VIII)
36° 30'
DALÍAS 1804 (IX)
-1000
-2000
Neogene-Quaternary basins
Neogene volcanics
External Zones
Malaguide complex
Alpujarride complex
Nevado-Filabride complex
Iberian Massif
-3° 30'
-3°

Figure 2.3. (previous page) a) Topographic and bathymetric map of the Eastern Betic Shear Zone (EBSZ). Topography is at 90 m grid spacing (SRTM web database) and bathymetry is at 70 m grid spacing (Gràcia et al., 2006; Ballesteros et al., 2008; Medimap, 2008). b) Geological map of the EBSZ (modified from Gràcia et al., 2006). The largest historical earthquakes (MSK Intensity > VIII) are depicted by black stars (IGN, 2010b). CrF: Crevillente Fault, BSF: Bajo Segura Fault, CaF: Carrascoy Fault, AMF: Alhama de Murcia Fault, AF: Albox Fault, PF: Palomares Fault, CF: Carboneras Fault.

Because of the wide scattering of deformation in the Eastern Betics, the release of accumulated elastic energy is generated through small faults (García-Mayordomo, 2005). The NW-SE trending fault systems such as the normal and dextral *Campo de Dalías* faults (Fig. 2.3a) are responsible for most of the present-day seismicity in the EBSZ (Rodríguez-Fernández and Martín-Penela, 1993; Sanz de Galdeano et al., 1995), which is consistent with the direction of the main convergence (NNW-SSE). The E-W and NE-SW oriented faults, such as the Bajo Segura and Carboneras faults, are inherited structures from previous stress field situations and are reactivated under the new stress field (Bousquet et al., 1976). At present, these structures accumulate stress during long periods of time, which implies a long recurrence and a high magnitude seismic cycle (Rodríguez-Fernández and Martín-Penela, 1993; Sanz de Galdeano et al., 1995).

2.3. The Carboneras Fault: background

The Carboneras Fault (Bousquet et al., 1975; Bousquet and Philip, 1976), also known as the Almería Fault (Baena et al., 1977; Weijermars, 1991) and Serrata Fault (Woodside and Maldonado, 1992; Estrada et al., 1997), is a left-lateral transpressive structure formed by several strands of subvertical traces extending at least up to the lower crust (maximum fragile break depth around 20 km after Torné et al. (2000), around 15-20 km after Pedrera et al. (2010), and around 12 km according to García-Mayordomo (2005)). The fault width varies from a single trace reaching the surface to about 2 km fault zone. The relief and intersection of "en-echelon" fault traces shows characteristic transpressive structures such as pressure-ridges, shutter-ridges, deflected drainage, sag-ponds, water gaps and en-echelon folds (Sylvester, 1988; McCalpin, 1996; Cunningham and Mann, 2007) observed both onshore (Moreno et al., 2007) and offshore (Gràcia et al., 2006). The sinistral character of the fault is evidenced by micro and macrostructures (Bousquet et al., 1975; Fournier, 1980; Rutter et al., 1986; Keller et al., 1995) along the fault zone. To the west, it delimits the extension of the volcanic province of the Gata Range (Bousquet et al., 1978), suggesting that it played a major role during the Neogene evolution of the area.

The CFZ has changed its kinematics from pure sinistral strike-slip to transpressive strike-slip following changes in the local stress field (e.g Fournier, 1980; Sanz de Galdeano, 1990) since its formation in the Early-to-Mid Miocene according to some authors (e.g. Fournier, 1980; Sanz de Galdeano, 1990; Scotney et al., 2000) or in the Late Miocene according to others (e.g. Weijermars, 1987; Vegas, 1992). Pedrera et al., (2010) propose that the nucleation of the fault could have occurred at the base of a thin crust, where melting processes critically reduced lithospheric strength during the late Miocene, to then propagate vertically upward, partially transferring deformation across the sub-horizontal crustal discontinuities and reaching the topographic surface. Northward, where the lithosphere was moderately stronger, the crustal discontinuities favored the development of kilometric amplitude folds, such as the Alhamilla Range antiform, instead of strike-slip faults. Marín-Lechado (2005) and Pedrera et al. (2006) studied the history of the activity of the CFZ through the analysis of brittle deformation structures, gravity and magnetic data. These authors suggest that during Tortonian (NW–SE compression) the stress field was incompatible with the activity of the NE–SW oriented CFZ (Fig. 2.4a). In this stage, the Alhamilla Range antiform (Fig. 2.3a,b) started to develop (Latest Tortonian–Earliest Messinian) and the volcanic activity was mainly concentrated in the Cabo de Gata region. Soon after the Early Messinian, the change to N-S to NNE–SSW compression could have activated the CFZ (Fig. 2.4b) with a moderate fault slip (according to the absence of clear displaced markers between the volcanism on each side of the fault). During the Pliocene (NW–SE compression)

open folds and faults are developed together with the activation of NW-SE striking normal faults orthogonal to the CFZ.

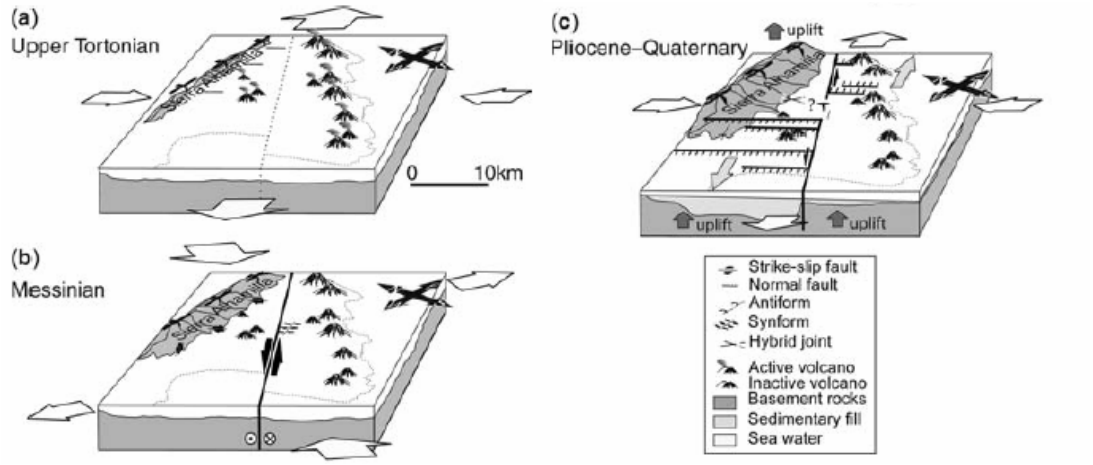

Figure 2.4. Block diagrams representing the evolution of the main structures and the regional stress field in the Almería–Níjar basin (Marín-Lechado, 2005; Pedrera et al., 2006).

At present, instrumental seismicity is minimal along the fault, while it is slightly more intense along the NW-SE trending normal faults of the Campo de Níjar and Dalías (IGN, 2010a). Martínez-Díaz (1998) and Marín-Lechado (2005) propose a connection between these two sets of faults despite discrepancies in the structural interpretation. Martínez-Díaz (1998) proposes a process of multi-fractured block escape (Fig. 2.5) consistent with the regional shortening where the NE–SW extensional features (Nijar basin and Campo Dalías depression) may be attributed to incompatibility problems due to relative movement and rotation of the blocks delimited by the Alhamilla and Gador ranges, which generates subsidence close to the CFZ (Fig. 2.5). On the other hand, Marín-Lechado (2005) proposes a tectonic model with normal faults dipping oppositely. The faults located in the occidental block of the CFZ dip to the SW and the faults located in the oriental block of the CFZ dip to the NE (Fig. 2.4c). These faults could be formed as a result of the SW extension of the occidental block and a NE extension of the oriental block. In this model, the CFZ which is orthogonal to both groups of faults, links the extension between the two blocks, acting as a transference fault and increasing its slip to the SW in the occidental block and to the NE in the oriental block. This model suggests a negligible slip in the central part. Nevertheless, field observations are not in line with this model that lacks slip in the central part of the onshore CFZ during the Pliocene and Quaternary.

Onshore, García-Mayordomo (2005) proposed 4 segments for the CFZ in accordance with the fault continuity, surface geomorphological expression, and the presence of N-S and NW-SE faults. From north to south: Carboneras, El Argamasón, La Serrata, and Rambla Morales, 10-12 km of length each (Fig. 2.3a). However, further

studies should determine whether these are real seismogenic segments capable of arresting the seismic rupture.

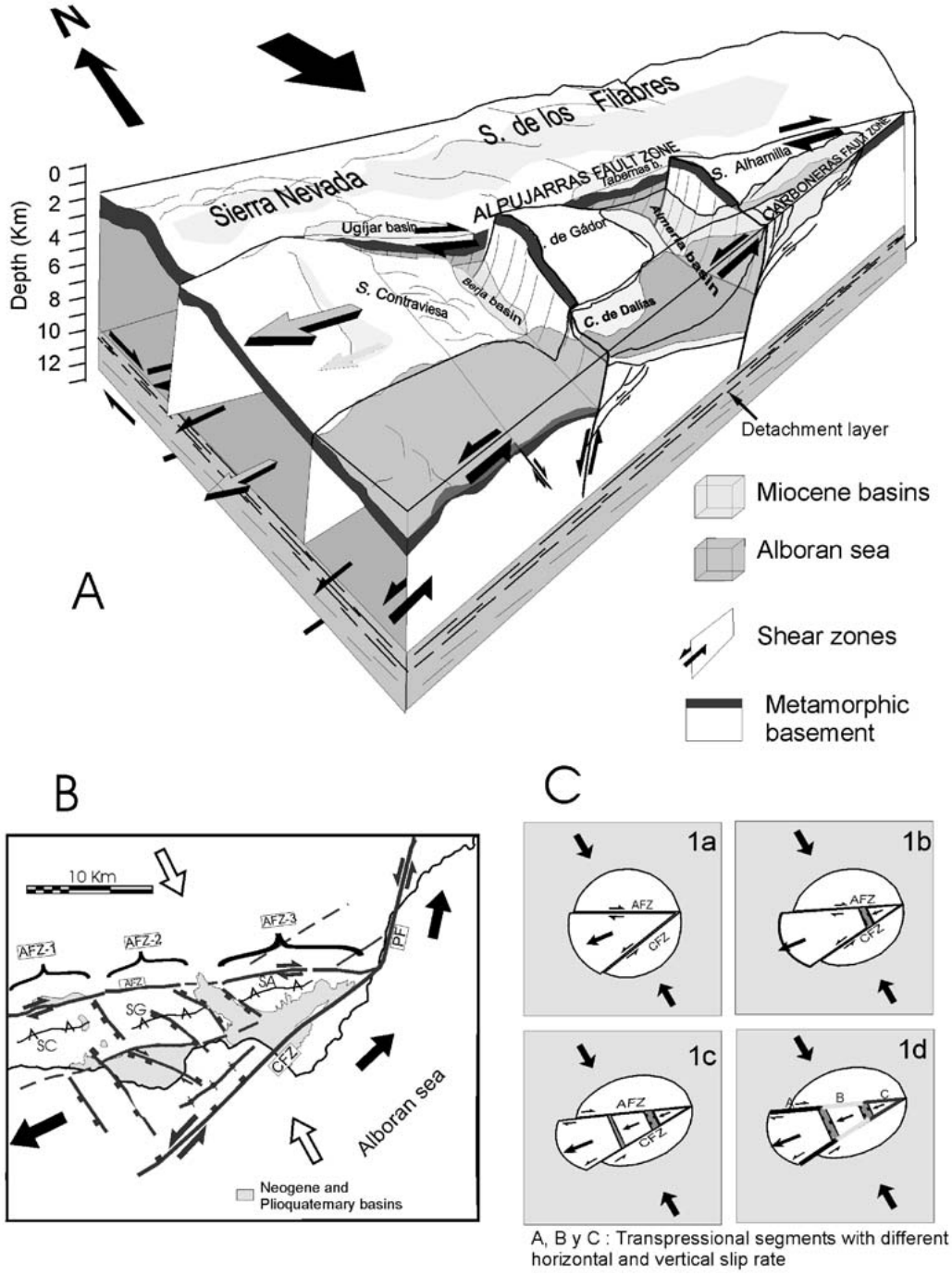

Figure 2.5. A) Model of block tectonics adapted to the morphology of the area limited by the Carboneras Fault Zone (CFZ) and the Alpujarras fault zone (AFZ). The extensional fault zones control the western flanks of Gador and Alhamilla ranges. They absorb the traction produced in the wedge by the strike-slip movement on AFZ and CFZ. B) Map view of the model pointing out the three segments of the Alpujarras fault zone with different horizontal slip rates driving the traction that could explain the tilting accounting for the present ranges: Contraviesa (SC), Gador (SG) and Alhamilla (SA). C) Simple model of the local extension produced by the wedge-shaped block escape (Martínez-Díaz and Hernández-Enrile, 2004).

To the southwest, the Carboneras Fault extends offshore along the continental shelf (Baena et al., 1982) for more than 100 km with clear evidence of surface rupture (Estrada et al., 1997; Reicherter and Hübscher, 2006; Gràcia et al., 2006). The first morphostructural reconnaissance of the Carboneras Fault offshore was carried out during the HITS-2001 cruise. During this cruise swath bathymetry, TOBI sidescan sonar mosaic (Fig. 2.6) and sub-bottom profiler across the Almería Margin were acquired (Gràcia et al., 2006). From this dataset, Gràcia et al. (2006) define two main segments on the basis of their fault orientation: a N045º trending segment starting onshore and ending at 36º30'N; and a N060º trending segment starting at 36º26'N and ending at 36º18'N (southern end of the fault). The two segments intersects an underlapping restraining step-over defined by a narrow (<1 km) arcuated ridge (ridge ER in Fig. 2.7) bounding an elongated depression (Gràcia et al., 2006).

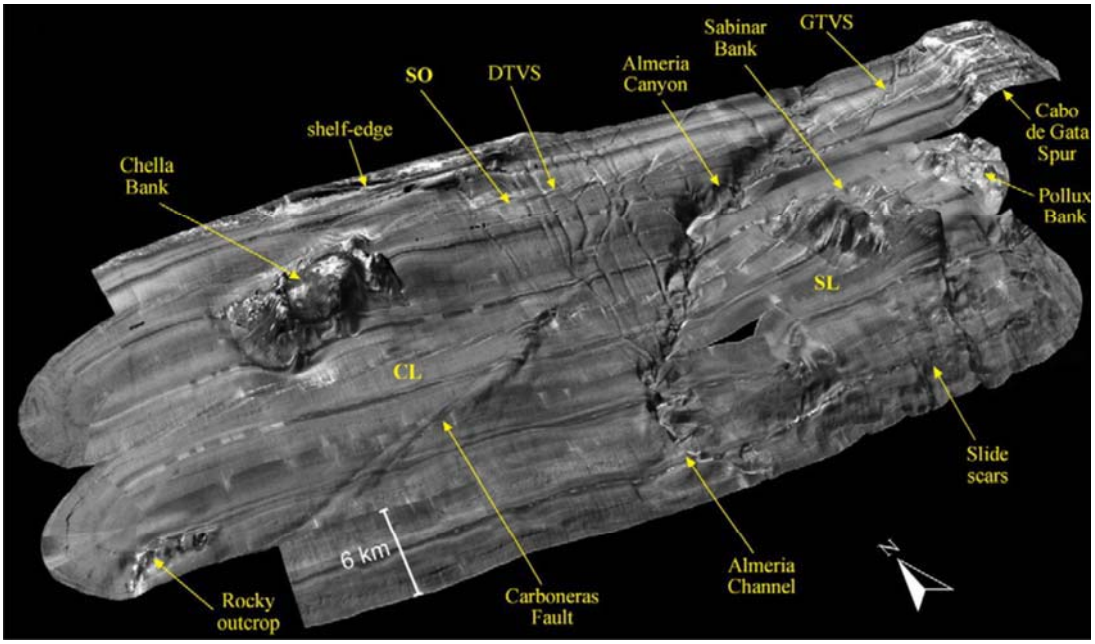

Figure 2.6. TOBI sidescan sonar overlapped on a 3D DTM model (vertical exaggeration 1:6) of the Almería Margin, surveyed during the HITS 2001. Main morphological features are located. Pixel resolution 6m. DTVS: Dalías Tributary Valley System; GTVS: Gata Tributary Valley System; SO: sediment overflowing; CL: Chella landslide; SL: Sabinar landslide (Gràcia et al., 2006; Lo Iacono et al., 2008).

The escarpment produced by the Carboneras Fault is clearly observed in the bathymetric images that correspond to a sharp backscatter contrast as shown in the TOBI sonographs (Fig. 2.6) (Lo Iacono et al., 2008). The elevation of the seafloor produced by the fault shows maximum local slopes of 16° at a depth of about 900 m (Fig. 2.7a). The Carboneras Fault gives rise to the sharp course deflection of the gullies from the DTVS (Fig. 2.6 and 2.7) (García et al., 2006). Most of the gullies are deflected for more than 2 km towards the SW when intersecting the Carboneras Fault Zone and in

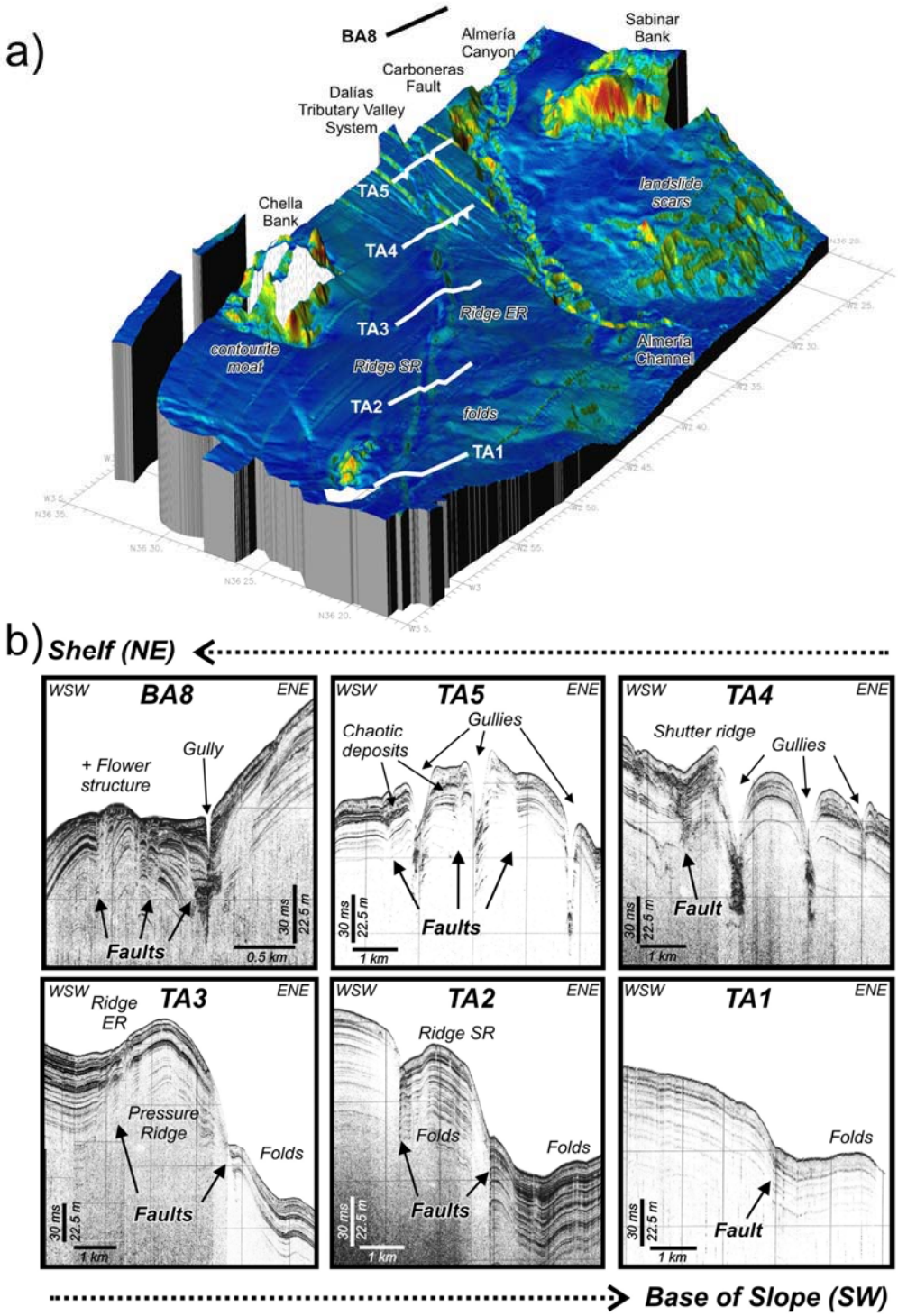

Figure 2.7. (a) Slope map superimposed onto 3D swath-bathymetry data of the Carboneras Fault zone, view from the southwest. The thick white lines depict location of profiles (BA8 to TA8) presented in (b). (b) Succession of high-resolution Sub-bottom (parametric echo-sounder) profiles across the Carboneras Fault zone from the shelf to the base of the slope depicting along-strike morphostructural variability. ER: arcuate elevated ridge, SR: Subdued ridge. Vertical scale in m is calculated by applying a velocity of sound propagation in water of 1500 m/s. Vertical exaggeration ~40, except for profile BA8, which is ~55 (Gràcia et al., 2006).

many places they bend sharply towards the SE (Gràcia et al., 2006). Thus, these gullies are deflected at the Carboneras Fault but they do not seem to be left-laterally offset by the fault. High-resolution sub-bottom profiles across the Carboneras Fault denote a considerable variability in the sub-surface structure of the fault (Reicherter and Hübscher, 2006; Gràcia et al., 2006). Folded and faulted Holocene sedimentary sequences provide evidence for the recent tectonic activity along this fault system (Fig. 2.7b). Near the shelf area, well-stratified units are folded and cut by sub-vertical faults forming a positive flower structure (profile BA8 in figure 2.7b). In the area intersecting the Dalías Tributary Valley System the Carboneras Fault zone presents a seafloor upwarp (profiles TA4 and TA5 in figure 2.7b). Further south, folded stratified units forms a pressure ridge (profile TA3 in figure 2.7b) (Gràcia et al., 2006).

2.4. Seismicity

2.4.1. Implications of fault gouges for the seismic behaviour of the Carboneras Fault

Studies on exposures of fault gouges (Fig.2.3a) in the northern segment of the Carboneras Fault (e.g. Rutter et al., 1986; Keller et al., 1995) have contributed to the controversy about the capability of this fault to produce large earthquakes as opposed to slipping continuously (creep) because of the low friction of the clays in the fault gouge. The best fault gouge exposure corresponds to a 50 m wide outcrop located at the intersection of the fault zone and the Rambla de Granatilla valley (Fig. 2.8), NW of the village of Carboneras (Fig. 2.3a). The fault gouges were created during the Miocene extensional stage by the sliding of the Maláguide nappe over the Alpujárride complex along low-angle faults that produced a considerable thinning of the thrust stacks (Alonso-Chaves et al., 2004). The Carboneras Fault intersected these materials and incorporated them into its fault plane. Then, the gouges could have been uplifted to shallower parts of the fault as a result of the transpressive movements. These clays would prevent the seismic behaviour of the fault if they were distributed along a large surface of the fault zone. This distribution along the fault zone is difficult to confirm since little subsrface information is available.

Figure 2.8. Fault gouge exposure at the intersection of the CFZ with the Rambla Granatilla Valley.

2.4.2. Historical seismicity

The Spanish seismic catalogue lists numerous catastrophic earthquakes, starting with archeoseismological evidence of an earthquake that occurred in the Pyrenees around year 800 BC (Martínez-Solares and Mezcua, 2002). Written records commenced about 1300 years ago (the VIII century). From these, it is inferred that most of the large historical earthquakes including five MSK I>IX destructive events occurred in the Betic

Ranges (Table 2.1), one of the most active zones in the Iberian Peninsula. The structures of the EBSZ are responsible for a number of large events since the XV century, such as those of Vera (AD 1518, I=VIII-IX), Almería (AD 1522, I=VIII-IX), Baza (AD 1531, I=VIII-IX), Dalías (AD 1804, I=VIII-IX) and Torrevieja (AD 1829, I=IX-X) (Martínez-Solares, 1995). The occurrence of these large earthquakes demonstrates the seismogenic nature of some faults. Nevertheless, other seismogenic structures may be unknown owing to their very long seismic cycles, perhaps one or two orders of magnitude longer than the time covered by the historical catalogue.

The town of Almería has historically been devastated by a number of earthquakes (AD 1487, AD 1522, AD 1659, AD 1804) (e.g. Udías et al., 1976; Bousquet, 1979), causing loss of life and collapse of buildings (Martínez-Solares, 1995; IGN, 2010b). Strike-slip motion along the Carboneras Fault could be the triggering mechanism for these earthquakes, especially for the AD 1522 earthquake (Fig. 2.9b) on the basis of tsunami deposits found in coastal lagoons near Cabo de Gata (Reicherter and Hübscher, 2006). However, the inaccurate location of these epicenters and the proximity of other seismogenic structures (for example the NW-SE trending faults) make it difficult to link these earthquakes with specific structures or fault segments. Further paleoseismic evidence is therefore needed to reveal the source of these historical earthquakes.

Table 2.1: List of the most important earthquakes in the Iberian Peninsula between years AD 1000 and AD 1900 (Martínez-Solares and Mezcua, 2002).

Date	Location	Coordinates	Maximum Intensity
1048	Orihuela (Alicante)	38º 05' N - 0º 55' W	VIII
1169	Andujar (Jaén)	38º 00' N - 4º 00' W	VIII-IX
1356-agosto-24	SW. Cabo San Vicente	36º 30' N - 10º 00' W	VIII
1373-marzo-2	Ribagorça (Lleida)	42º 30' N - 0º 45' E	VIII-IX
1396-diciembre-18	Tavernes de la Valldigna (Valencia)	39º 05' N - 0º 13' W	VIII-IX
1427-mayo-15	Olot (Girona)	42º 12' N - 2º 30' E	VIII-IX
1428-febrero-2	Queralbs (Girona)	42º 21' N - 2º 10' E	IX-X
1431-abril-24	Sur de Granada	37º 08' N - 3º 38' W	VIII-IX
1494-enero-26	Sur de Málaga	36º 35' N - 4º 20' W	VIII
1504-abril-5	Carmona (Sevilla)	37º 23' N - 5º 28' W	VIII-IX
1518-noviembre-9	Vera (Almería)	37º 14' N - 1º 52' W	VIII-IX
1522-septiembre-22	W. Alhama de Almería	36º 58' N - 2º 40' W	VIII-IX
1531-enero-26	Vila Franca de Xira (Portugal)	39º 00' N - 8º 55' W	IX
1531-septiembre-30	Baza (Granada)	37º 32' N - 2º 44' W	VIII-IX
1644-junio-19	Muro de Alcoy (Alicante)	38º 48' N - 0º 25' W	VIII
1658-diciembre-31	Almería	36º 50' N - 2º 28' W	VIII
1680-octubre-9	NW. Málaga	36º 48' N - 4º 36' W	VIII-IX
1722-diciembre-27	Golfo de Cádiz	36º 24' N - 7º 46' W	VIII
1748-marzo-23	Estubeny (Valencia)	39º 02' N - 0º 38' W	IX
1755-noviembre-1	SW. Cabo San Vicente	36º 30' N - 10º 00' W	X
1804-agosto-25	Dalías (Almería)	36º 46' N - 2º 50' W	VIII-IX
1806-octubre-27	Pinos Puente (Granada)	37º 14' N - 3º 44' W	VIII
1829-marzo-21	Torrevieja (Alicante)	38º 05' N - 0º 41' W	IX-X
1858-noviembre-11	S. Setúbal (Portugal)	38º 18' N - 8º 55' W	IX
1884-diciembre-25	Arenas del Rey (Granada)	37º 00' N - 3º 59' W	IX-X

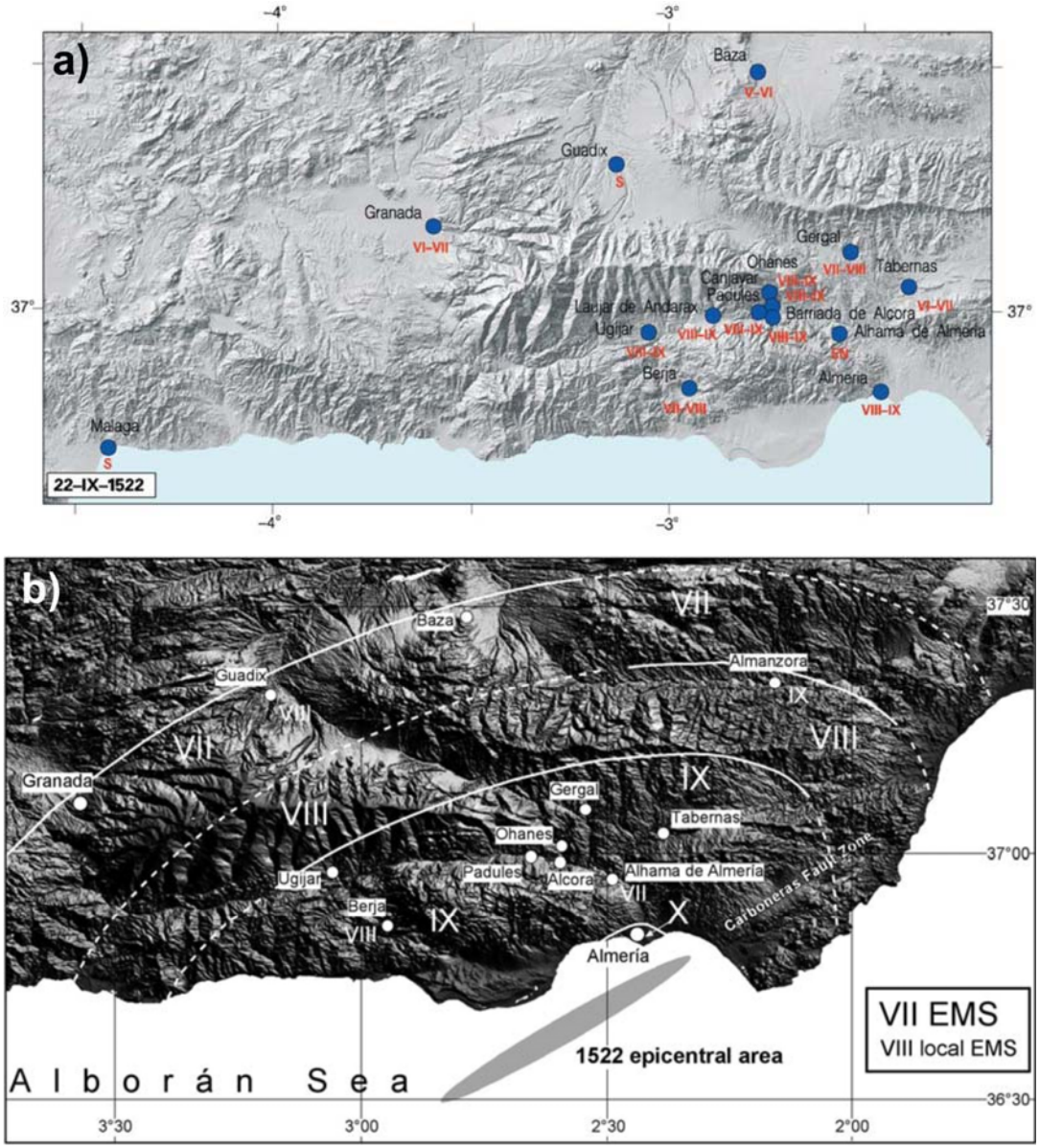

Figure 2.9. a) Macroseismal information of the 1522 Almería earthquake (Martínez-Solares and Mezcua, 2002). b) Digital elevation model of the eastern Betic Cordilleras and the Cabo de Gata block with isoseismals of the 1522 Almería earthquake constructed after damage reports (López Marinas, 1985; Martínez-Solares, 1995) (Reicherter and Becker-Heidmann, 2009).

2.4.3. Instrumental seismicity

The seismicity in the Ibero-Maghrebian region is spread over a wide zone, and does not clearly delineate the European-African plate boundary (Buforn et al., 1995; Morel and Meghraoui, 1996) (Fig. 2.10). The main seismic domains are divided into the Iberian Massif, offshore southern Portugal, the Alboran Sea, Northern Algeria and Southeastern Spain (Stich et al., 2003). In the southeastern Iberian Margin, instrumental seismicity is characterized by continuous, shallow seismic events of low to moderate

magnitude responding to a heterogeneous faulting regime, from normal to reverse (Udías et al., 1976; Buforn et al., 1995; Stich et al., 2003; IGN, 2010b).

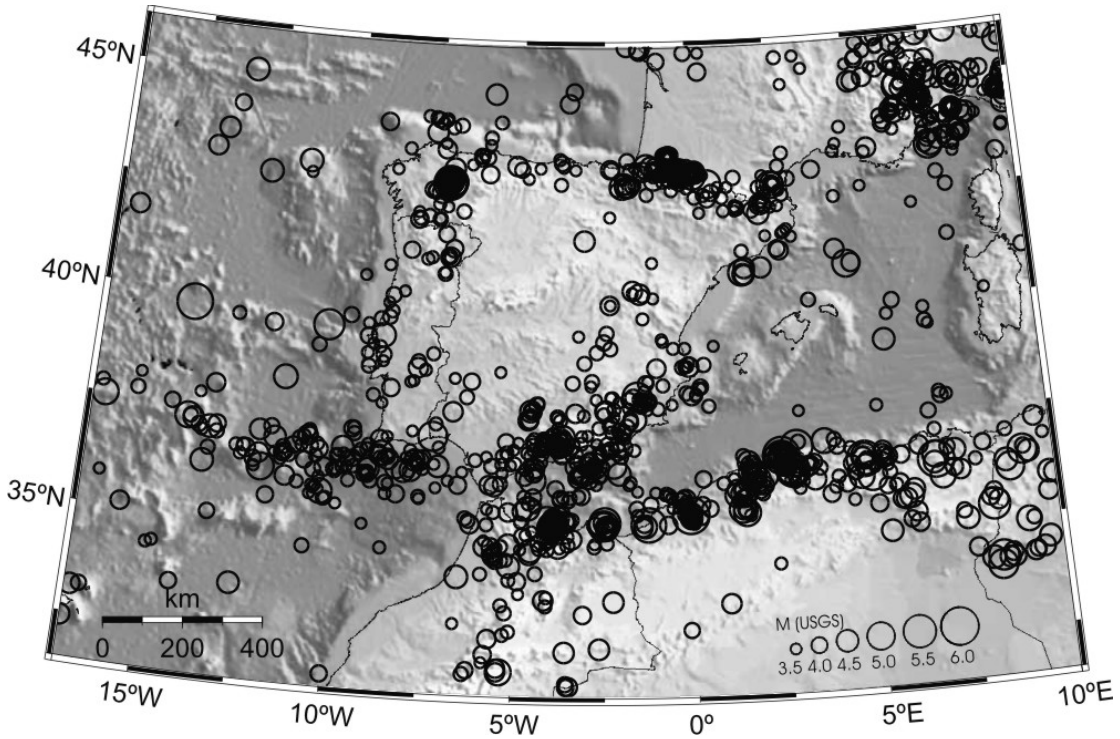

Figure 2.10. Distribution of small to moderate seismicity in the Ibero-Maghreb region ($m_b \geq 3.5$) for the 20-year period March 1982 to March 2002 (USGS/NEIC data file) (Stich et al., 2003).

The kinematics of the active faults of the southeastern Iberian Margin is evidenced by earthquake mechanisms derived from moment tensor inversion (Buforn et al., 1995; Stich et al., 2006; Stich et al., 2010) (Fig. 2.11). Along the EBSZ and the Alboran Sea, strike-slip faulting dominates (Stich et al., 2003) as corroborated by geological and geophysical data (Bousquet, 1979; Silva et al., 1993; Comas et al., 1999; Alvarez-Marrón, 1999; Masana et al., 2004; Martínez-Díaz and Hernández-Enrile, 2004) (Fig. 2.11). The 1910 Adra seismic series, the largest instrumentally-recorded crustal earthquake in Spain with a maximum magnitude Mw 6.1, demonstrates the present-day active seismicity in the area. Recently, the Lorca earthquake on 11 May 2011, with a main-shock of Mw 5.1, located only at 2 to 6 km depth, caused fatalities and considerable damage to buildings. The seismic waves were probably amplified by large site-effects, producing unexpected peak ground accelerations in Lorca and turning this earthquake into a catastrophic one. This event confirms the present-day seismic activity and hazardous nature of the structures along the EBSZ.

As for the instrumental seismicity around the CFZ, very few earthquakes have been recorded along the fault trace, all of them of low to moderate magnitude. The lack of large seismic events in the last half century suggests an increase in accumulated

strain, enhancing the seismic potential of the fault. There is consequently a pressing need for obtaining slip-rates across the fault.

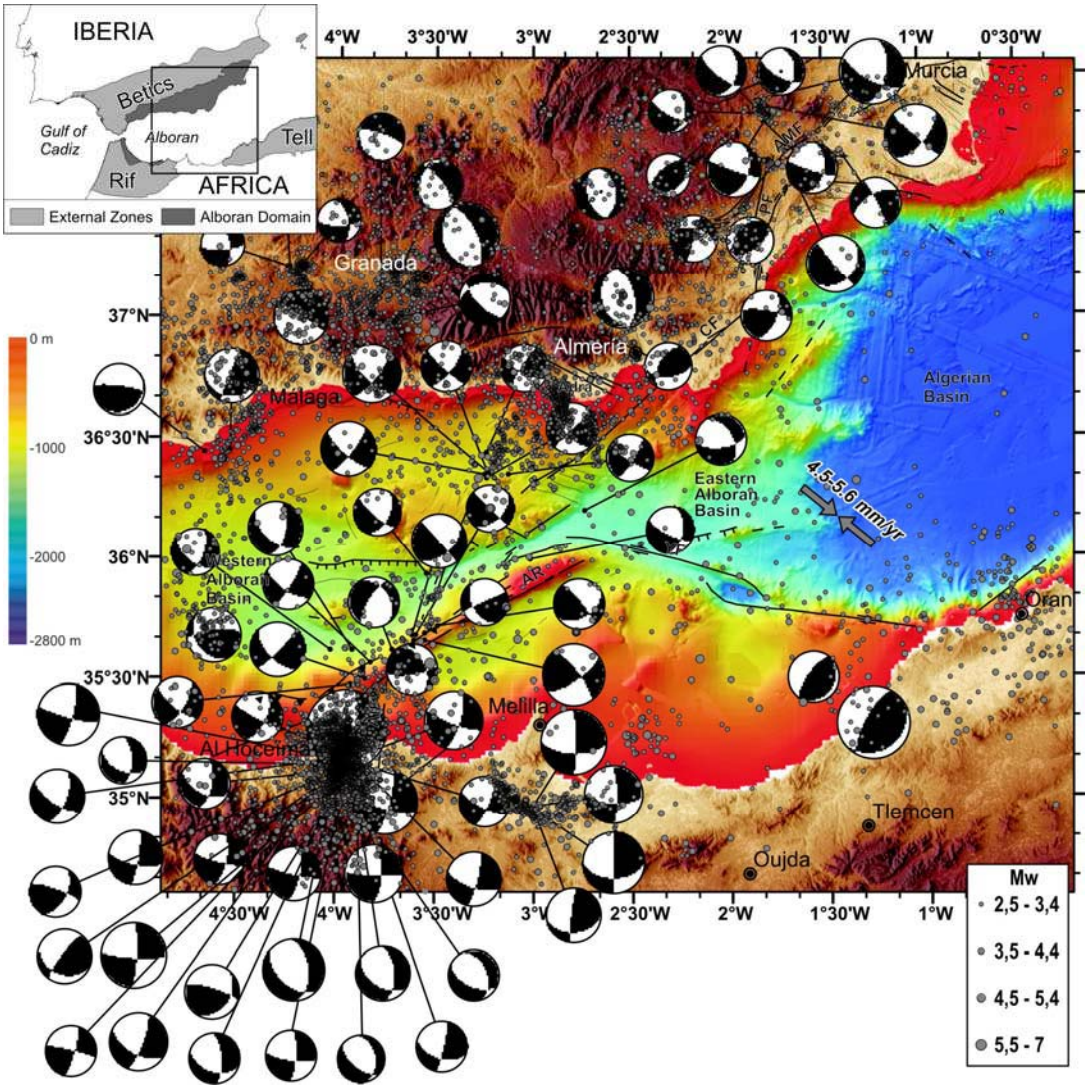

Figure 2.11. Instrumental seismicity (IGN, 2010b) and focal mechanisms (Stich et al., 2006) of the area embracing the southeastern Iberian Peninsula and north Africa. Topography is at 90 m grid spacing (SRTM web database) and bathymetry is at 70 m grid spacing (Gràcia et al., 2006; MEDIMAP Group et al., 2008; Ballesteros et al., 2008). Inset: Location of the study area in the EBSZ. Grey arrows show the direction of convergence between the Eurasian and African plates from NUVEL1 model (Argus et al., 1989; DeMets et al., 1990).

2.5. Previous paleoseismic results in the Eastern Betic Shear Zone

The low convergence rates between the Iberian and African plates suggest that the faults from the EBSZ responds to slow movements (Masana et al., 2010). Recent paleoseismic and geological studies have demonstrated this. The most significant paleoseismic results from the main faults of the EBSZ are summarized below:

2.5.1. Bajo Segura Fault

The activity in this fault started during the Early Pleistocene and continued up to the Holocene (Alfaro et al., 2002a; Alfaro et al., 2002b) with maximum uplift rates for several folds between 0.1-0.3 mm/a (Taboada et al., 1993). In this area, up to seven seismite levels have been recognized from sediment cores, dated as younger of 8000 years and most probably caused by the Bajo Segura Fault, although other smaller faults, such as the Torrevieja Fault and San Miguel de Salinas Fault cannot be ruled out. The recurrence period of earthquakes (Mw>6) of 1000 years is calculated for the area on the basis of these seismic deposits (Alfaro et al., 2001). The Bajo Segura anticline continues underwater through the Alicante shelf towards the ENE at least 60 km sin-tectonically controlling the growth of Quaternary deposits. Up to 13 sedimentary unconformities in a folded and faulted Quaternary sequence are described using high-resolution Sparker seismic profiles. The results show no recent deformation along the San Miguel de Salinas Fault but indicate seafloor rupture along several faults that constitute the offshore continuation of the Bajo Segura Fault (Perea et al., 2010).

2.5.2. Carrascoy Fault

The lack of evidence of recent activity in the part of the AMF running parallel to the CaF suggests a relay of the deformation concentrating it into the CaF. Geomorphologic anomalies, such as gully deflections or fault scarps on Upper Pleistocene-to-Holocene deposits, provide evidence of the recent tectonic activity of the Carrascoy Fault. A strike-slip rate of 0.5-1 mm/a has been inferred from the 90-220 m displacement of gullies in the last 160 ka (Silva, 1994).

2.5.3. Alhama de Murcia Fault / Albox Fault

This fault has a sinistral movement with a local reverse component (Bousquet and Montenat, 1974). The neotectonic activity of the Alhama de Murcia Fault is well illustrated by its morphology (triangular facets, aligned valleys, sudden changes in the entrenchment of the creeks along the fault, etc.) (Masana et al., 2010). The Alhama de Murcia Fault has been divided into five segments, from north to south, on the basis of tectonic-geomorphological features and distribution of seismic activity: Alcantarilla-

Alhama (23 km); Alhama-Totana (12 km); Totana-Lorca (23 km); Lorca-Puerto Lumbreras (30 km); Puerto Lumbreras-Góñar (12 km) (Fig. 2.3a) (Martínez-Díaz, 1998; Masana et al., 2005; Ortuño et al., In prep.). To the SW of the Puerto Lumbreras-Góñar segment, the AMF Plio-Quaternary activity is transferred to E-W oriented faults and folds outcropping at the southern boundary of the Las Estancias range and in the Huercal-Overa depression (Fig.2.3a,b). Of these faults, the Albox fault is the only one to which seismogenic behaviour has been ascribed so far (Masana et al., 2005) and thus it is assumed to be absorbing the southern movement of the block west of the AMF (Soler et al., 2003; Masana et al., 2004; Masana et al., 2005).

Paleoseismic studies have been carried out along the Totana-Lorca and Puerto Lumbreras-Goñar segments and also along the reverse ENE-WSW Albox fault. In the Totana-Lorca segment, the fault is divided into two strands, one of which dips to the east and blocks the drainage of the fans towards the Guadalentin depression. Four trenches have been dug and analyzed in two different sites revealing the seismogenic behaviour of the fault (Martínez-Díaz et al., 2003; Masana et al., 2004). Evidence for three paleoearthquakes for the last 27 ka was found, the last event being very recent (around AD 1650) and a recurrence period of 14 ka is estimated. The integration of the paleoseismic results suggests dip-slip rates of 0.12-0.16 mm/a for the last 23.8 +/-3.1 ka and 0.04-0.06 mm/a for the last 17.2 +/-2.3 ka (Martínez-Díaz et al., 2001; Masana et al., 2004). Moreover, Mid Pleistocene alluvial fans draining from the La Tercia Range are folded (Silva, 1994) and the deformation is constrained downwards and upwards by travertines dated with U/Th, suggesting 0.08-0.09 mm/a of maximum dip-slip rate (Martínez-Díaz and Hernández-Enrile, 2001). The poorly constrained horizontal slip of the Lorca Totana segment has been inferred from deflected river courses (*ramblas*) with average displacements of 26.7 m. Estimating the beginning of these deformations during the Upper Pleistocene (125 ka), Martínez Díaz et al., (2003) obtain a 0.21 mm/a strike-slip rate. On the basis of the orientation of striations, Masana et al. (2004) suggest a left-lateral/reverse slip and estimates the net slip-rates in 0.07-0.66 mm/yr for the last 30 ka, divided into 0.04-0.35 mm/yr of vertical slip-rate and 0.06-0.53 mm/yr of strike-slip rate.

Silva et al. (2003) obtained Quaternary uplift rates of 0.08-0.15 mm/a after comparing the geomorphological characteristics of Puerto Lumbreras mountain front with those of other mountains of the SE Iberian Peninsula. In the Lorca-Puerto Lumbreras segment, left-lateral offsets in Upper Pleistocene channels have been observed, ranging from 25 to 75 m (Silva, 1994). Given that the channels have been active for the last 125 ka, maximum strike-slip rates of 0.2-0.6 mm/a are obtained.

The southern end of the Alhama de Murcia Fault, in the Puerto Lumbreras-Goñar segment, splays into an array of ENE-WSW trending faults and folds showing a complex horse-tail termination structure (Fig. 2.3a,b) that cuts through the Quaternary

alluvial fans in the Goñar area. The geomorphology shows recent activity along most of these faults such as left-lateral deflection of channels or blockage of alluvial fans. Trenching at six sites distributed along the different traces of the fault showed evidence of a minimum of 9 paleo-earthquakes affecting the area during the Late- Pleistocene, with 0.8 m of maximum dip slip per per event. Finally, the 6 km long system suggests that a maximum Mw= 7 can occur in the area (Ortuño et al., 2010; Ortuño et al., In prep.).

To the southwest, the Albox Fault cuts the Neogene to Quaternary Huercal-Overa depression (Fig. 2.3a). This is an ENE-WSW-trending reverse fault that strongly dips to the north. Quaternary alluvial fans draining from the Las Estancias range to the south towards the Huercal-Overa depression have been observed to be deformed by this fault (Soler et al., 2003; García-Meléndez et al., 2004). Trenches dug across the fault at two sites provide evidence for two paleoearthquakes that probably occurred between the XVIII century and AD 650. The youngest was small in magnitude (few centimetres of vertical offset) and occurred shortly after AD 660 (Masana et al., 2005).

Given the slip per event, the maximum earthquake magnitude at Albox Fault has been considered to be Mw 6.5 and 7.0 at Goñar and at Lorca-Totana segments respectively. If the total length of the AMF (approximately 100 km) is taken into account, a maximum magnitude of Mw 8 can be achieved, considering a seismogenic depth of 15 km. However, this is not likely because the two northern segments show very little geomorphological expression of recent activity (Masana et al., 2010).

The large uncertainties associated with the slip rates obtained along the AMF do not allow us to accurately evaluate the distribution of the slip across the system or its variation with time. By contrast, they demonstrate the need for further numerical dates for the markers displaced as well as for more complete structural studies to quantify the net displacement along the system.

2.5.4. Palomares Fault

Lower to Upper Pleistocene deposits have been shown to be deformed by the PF (Wenzens and Wenzens, 1997; Silva et al., 1997). Silva et al. (1997) describe 1.8 m to 2.5 m high fault scarps in Early-Mid Pleistocene and Late Pleistocene alluvial fans, suggesting maximum dip-slip rates of 0.01-0.02 mm/a for the last 125 ka (García-Mayordomo, 2005). The tectonic activity of the Palomares Fault gradually decreases towards the north.

2.5.5. The Carboneras Fault

The Carboneras Fault Zone (CFZ) provides geomorphoogical evidence of Quaternary activity (e.g. Baena et al., 1977; Goy and Zazo, 1983; Harvey, 1990; Woodside and Maldonado, 1992; Boorsma, 1992; Keller et al., 1995; Estrada et al., 1997; Silva et al., 2003; Martínez-Díaz and Hernández-Enrile, 2004; Marín-Lechado, 2005; Reicherter and Hübscher, 2006; Gràcia et al., 2006). The long-term horizontal slip for the Carboneras Fault has also been discussed in the early studies of the fault. Hall (1983) proposed 5-6 km of vertical slip and 35-40 km of strike-slip for the CFZ between the Burdigalian and the present (1.7-2.5 mm/a), which is in agreement with apparently displaced volcanic rocks observed by Montenat and Ott D'Estevou (1996) and Rutter et al. (1986). Moreover, Montenat et al. (1990) described an 18 km displaced olistrostrome (*"brèche rouge"*) along the Carboneras Fault Zone. The olistrostrome was formed during the Late Tortonian/early Messinian and a minimum 2 mm/a strike-slip rate is inferred.

At the NE intersection of the CFZ with the shoreline, Thyrrenian marine terraces show apparently normal displacements (Goy and Zazo, 1986). These terraces of ca. 100 ka are vertically displaced 5 m (Bell et al., 1997), suggesting a dip-slip rate of 0.05 mm/a. In the same area, Reicherter and Reiss (2001) observe in GPR profiles near-surface deformations in ca. 85 ka Thyrrenian (T-IV) marine terraces produced by small reverse and normal faults displaying positive and negative flower structures (typical of strike-slip motion). These observations provide evidence of an Upper Pleistocene activity in this segment of the CFZ. Further south, close to the village of El Argamasón, where the Alias River crosses the fault (Fig. 2.3a), a strongly cemented Quaternary river terrace is folded and faulted (Bousquet, 1979).

In the central part of the onshore Carboneras Fault Zone, in the La Serrata section (Fig. 2.3a), recent tectonic activity is evidenced by the relative disposition of alluvial fans and 80-100 m left-lateral deflected drainages (Bousquet, 1979; Goy and Zazo, 1986; Keller et al., 1995; Bell et al., 1997) (Fig. 2.12). Bell et al. (1997) suggest that these displacements took place at least since 100 ka BP, most probably during the Mid Pleistocene (125-700 ka). Assuming an average of 500 ka, the obtained strike-slip rate was 0.2-0.3 mm/a. Bell et al. (1997) find no evidence of movements younger than 100-35 ka, which is in agreement with Reicherter and Reiss (2001), who used high-resolution geophysical prospecting along several segments of the fault.

At the mouth of Rambla Morales, in the SW onshore boundary of the fault, normal movements are evidenced by slickensides in faults cutting Thyrrenian marine terraces. Assuming an age of ca. 100 ka for these terraces (Goy and Zazo, 1986) and a total slip between 5-10 m, a dip-slip rate around 0.05-0.10 mm/a has been suggested (Bell et al., 1997).

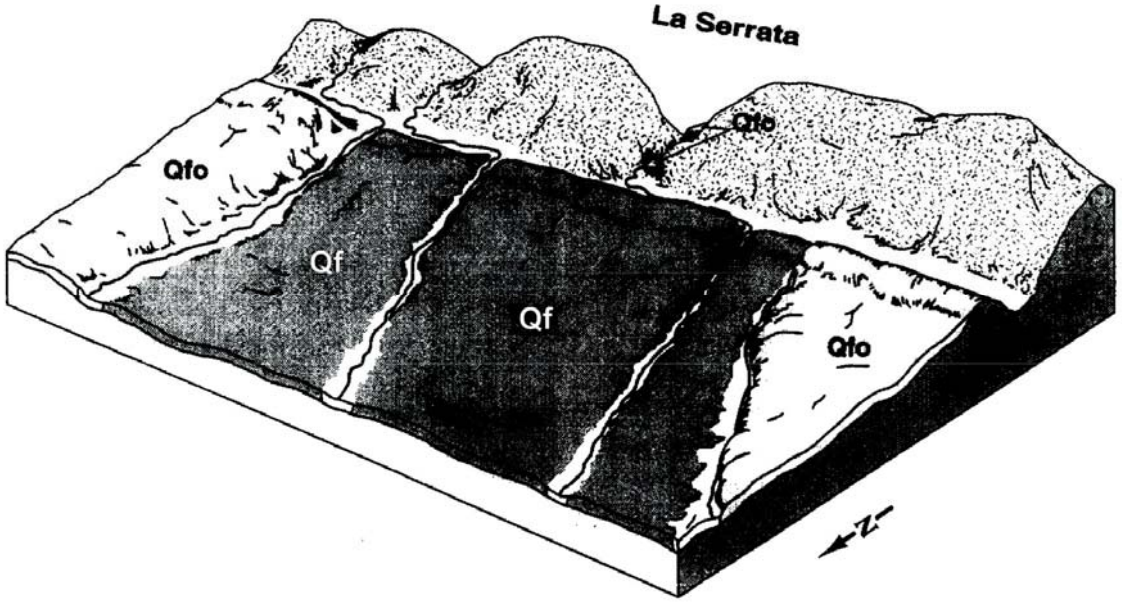

Figure 2.12. Three-dimensional isometric drawing of the northwest flank of La Serrata showing three offset stream channels and piedmont alluvium relations. Qfo: pre-Tyrrhenian alluvial-fan deposits (> 100 ka); Qf: post-Tyrrhenian alluvial-fan deposits (< 100 ka) (Bell et al., 1997).

Few studies have focused on the submerged portion of the CFZ. Estrada et al. (1997) described a flower structure affecting the Quaternary units based on single-channel seismics (Fig. 2.13). The CF offshore was first mapped in 2001 by Gràcia et al. (2006) using swath-bathymetry, sidescan sonar TOBI and parametric echo-sounder. Structures typically found on active transpressional fault systems were imaged. Using these data, these authors propose two geomorphic segments for the CFZ, a N045º segment hosting the onshore part and extending underwater for 33 km, and a 26 km long N060º segment. With this onshore-offshore segmentation, these authors suggest a maximum earthquake magnitude of Mw 7.4 (Gràcia et al., 2006). Reicherter and Hübscher (2006) used high-resolution seismic data (sediment profiler) across the northern segment of the CFZ and observed sedimentary and tectonic features, confirming the Late Pleistocene tectonic activity of the fault. Moreover, these authors propose that the seafloor ruptures along the CFZ are attributed to the AD 1522 Almería earthquake. Nevertheless, higher resolution and direct observations are needed to confirm the age of these apparent fresh ruptures, and dating is required to precisely constrain their ages in order to assign the ruptures to a historical event. This is essential when considering other nearby structures that are possible candidates, such as the onshore-offshore NW-SE normal faults located W of Almería, for being the source of this event (Masana et al., 2010).

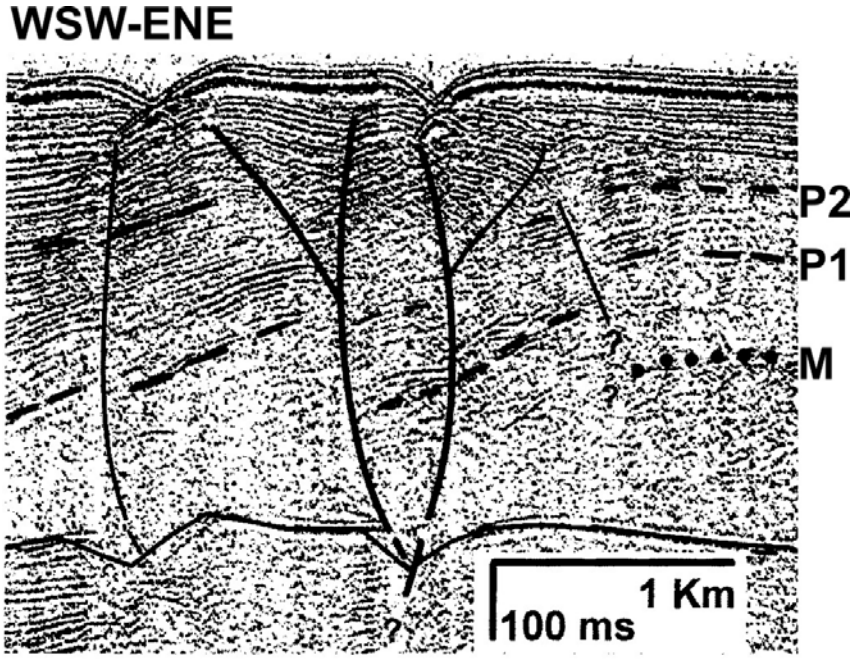

Figure 2.13. Flower structure across the Carboneras Fault Zone offshore observed through single-channel seismics. P2 reflection limits the Pliocene and Quaternary seismic units, P1 reflection limits de Lower and Upper Pliocene seismic units, and the M reflection is the erosive unconformity at the top of the Miocene seismic units (Estrada et al., 1997).

Bell et al., (1997) have also analyzed some deformation structures in the marine terraces all along the coastline between Cabo de Gata and Carboneras. These authors identified beach platforms, elevated 2-3 m above sea level with little erosion, which suggests a young Holocene age. Goy et al. (2003) have shown that the sea-level in the area has not risen more than 1 m or descended more than 0.5 m in the last 7400 years and has been similar to the present-day sea level for the last 500 yrs. Thus, a coastal uplift is inferred from this raised beach platform, supported by a young raised fluvial terrace whose base level is approximately coincident with the beach platform high. The age of the uplift might be close to the age of the fluvial terrace, dated to AD 1475 (+175/-50). The authors consider that this coastal uplift is caused by a seismic event, probably coinciding with the AD 1518 Vera or the AD 1522 Almería earthquakes. However, they do not assign this event to a specific fault, although the CFZ is the largest structure in the area.

The large uncertainties in the amount and age of the movements observed along the CFZ might lead to an under-evaluation of its Quaternary tectonic activity because of underestimating the slip-rates. Further and more complete paleoseismic studies are necessary for a more reliable estimation of the potential seismic hazard of this structure in the area.

2.6. The CuaTeNEo GPS network

The CuaTeNeo (*Cuantificación de la Tectónica y Neotectónica en parte de la Península Ibérica*) GPS network, which was set up in 1996 and was specifically designed to study the present-day crustal deformation in the SE part of the Betics (Castellote et al., 1997), helps to assess and complement the paleoseismic studies over a larger area. The network consists of 15 concrete geodetic monuments with embedded screws for the antennas distributed between Murcia and Almería. The results of measurements in 1997, 2002 and 2006 suggest that the estimated deformation field is relatively low and does not exceed 2 mm/yr when viewed in the fixed Eurasia frame. In general, the calculated velocity field provides evidence of localized deformations ascribed to the existing active faults within the area (e.g. Alhama de Murcia faults) (Khazaradze et al., 2008). In December 2008 and in the framework of the EVENT project, a continuous GPS station (GATA CGPS) was installed to the SW of the village of Rodalquilar, to monitor the activity of the Carboneras fault. Preliminary results of 15 month of long time-series suggest that the CFZ is moving and exhibits mainly left-lateral strike-slip motion of 1.5±0.7 mm/yr with a minor compressive component of 1.0±0.7 mm/yr (Fig. 2.14) (Khazaradze et al., 2010).

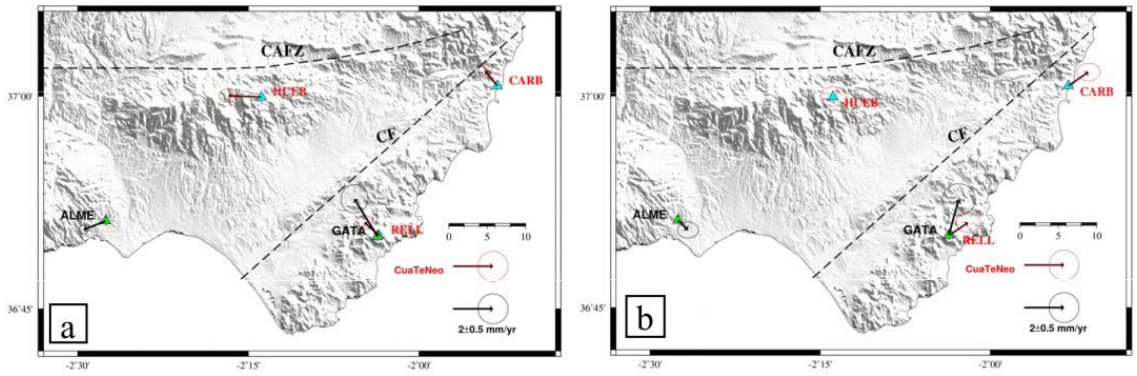

Figure 2.14. GPS Velocity vectors in mm/yr with 1σ errors. Red labels depict stations from CuaTeNeo GPS network (see Khazaradze et al. (2008) for more details). CF: Carboneras Fault; CAFZ: Corredor de las Alpujarras Fault Zone. a) Eurasia fixed referent frame; b) HUEB fixed reference frame (Khazaradze et al., 2010).

Chapter 3: Methods

Paleoseismology, like most empirical sciences, demands a multidisciplinary and multi-scale approach to obtain consistent results. This is even more evident when the fault studied runs onshore and continues offshore. Sub-aqueous paleoseismology represents a unique and powerful integration technique that complements the continuous Holocene faulting register with the paleoseismic knowledge already existing onland (Pantosti and Gràcia, 2010). Indirect geophysical methods are indispensable in marine environments, although they are also extensively used onshore, providing a large coverage acquired easily in a relatively short time and with different degrees of resolution. Marine sedimentation is generally continuous in time and space, allowing for regional stratigraphic correlations and for the reconstruction of a complete record of events. Moreover offshore regions are essentially free of human modification preventing the full application of paleoseismology (Pantosti and Gràcia, 2010). On the other hand, direct or *in situ* analyses, such as trenches, are more widely used in onshore studies, providing hands-on observations such as differentiating events. The study of onshore-offshore structures is challenging as it requires expertise in different methodologies in order to obtain a more accurate understanding of the fault. However, it has the advantage of combining good fault preservation, *in situ* fault measurements and the long temporal span obtained from offshore records.

The descriptions of the methods used in this study are divided into two main categories depending on whether techniques are used for an indirect or direct analysis. Indirect study techniques are separated into the analysis of the landforms (section 3.1.1) and the analysis of the stratigraphic features (section 3.1.2).

3.1. Indirect techniques

3.1.1. Surface analysis (geomorphological evidence)

The geomorphological analysis of the area around the fault constitutes a good first approach to the interaction between the fault and the ground surface, and therefore to the recent activity of the fault. In consequence, landsurface is meticulously analysed in paleoseismic studies to identify the geomorphic evidence of active faults, such as seafloor ruptures, folds or fault scarps. During the past decades, as a result of the digital revolution, the Earth's surface has been increasingly analysed with indirect techniques, allowing a rapid bird's eye-view of large areas around fault traces and associated features. Nowadays, the observation of the land surface is mostly done through

numerical analysis. Numerical data are processed to obtain models showing different kinds of information, such as surface relief, slope maps or satellite images. This large amount of information is now manageable thanks to the geographic information systems that enable us to visualize (in 2D or 3D) and merge our dataset. For this study, commercial softwares as *Fledermaus 7* (IVS 3D), *ArcGIS 9.3* (ESRI) and *Cartomap 5.0* (ANEBA) were recurrently used.

3.1.1.1. Digital Elevation Models (DEM)

A DEM is a regularly spaced grid file with elevation information posted at every point. Through the processing of this grid file we obtain a digital representation of the ground surface (McCalpin, 2009). Onshore, DEMs are commonly built using remote sensing techniques, such as satellite or airplane surveys. The DEM used in this study comes from the *Consejería de Medio Ambiente* of the *Junta de Andalucía* and has a 10 m spaced regular grid. The DEM was incorporated into the *ArcGIS* software and used to produce contour lines, slope maps, and shaded maps of the onland topography. The same DEM was incorporated into the *Fledermaus* software to make a 3D exploration of the topographic mosaic.

3.1.1.2. Swath-bathymetry and acoustic backscatter

Bathymetric maps are DEMs acquired by multibeam sonars onboard research vessels by sending an acoustic signal that is reflected on the seafloor and is recovered back by tens of transducers located at the hull of the vessel. The recovered signal provides both elevation (bathymetry) and backscatter strength of seafloor materials, which is a function of the angle of incidence, slope, and material properties (grain size, hardness, etc). The swath coverage is proportional to the water depth, obtaining restrained coverage in shallow waters and larger swath in deeper waters.

The first swath-bathymetric map of the Almería margin was obtained using the Simrad EM12 (Table 3.1, Fig. 3.1) during the HITS cruise onboard the BIO Hespérides, mainly devoted to a TOBI sidescan sonar recognition of the area (Gràcia et al., 2006; Lo Iacono et al., 2008). During the IMPULS survey the new Simrad EM120 multibeam echo-sounder of the BIO Hespérides (Diez and Gràcia, 2005) was used simultaneously with the seismic survey, and thus, the coverage area spans about 7-11 miles around the Carboneras Fault area. To complete the bathymetry of the entire Almería margin, data from the *Instituto Español de Oceanografía* (IEO) was incorporated (Table 3.1, Fig. 3.1). The IEO swath-bathymetric data for the shelf area was acquired during the ESPACE project (*Estudio de la Plataforma continental Española*) in 2000 onboard the RV Miki I and in 2003 onboard the RV Teresa Rosa. Both surveys used a Simrad EM3000 dual multibeam echo-sounder (Sanz et al., 2003). The IEO data for the deeper

parts of the Almería Margin was acquired during three campaigns (*500 viviendas*, *Alborán-02* and *Alborán-03*) onboard the RV Vizconde de Eza using always a Simrad EM300 (Muñoz et al., 2008; Ballesteros et al., 2008). XBT (eXpendable BathyThermograph) stations were systematically deployed to calibrate sound velocity profiles (SVP) during all the bathymetric surveys.

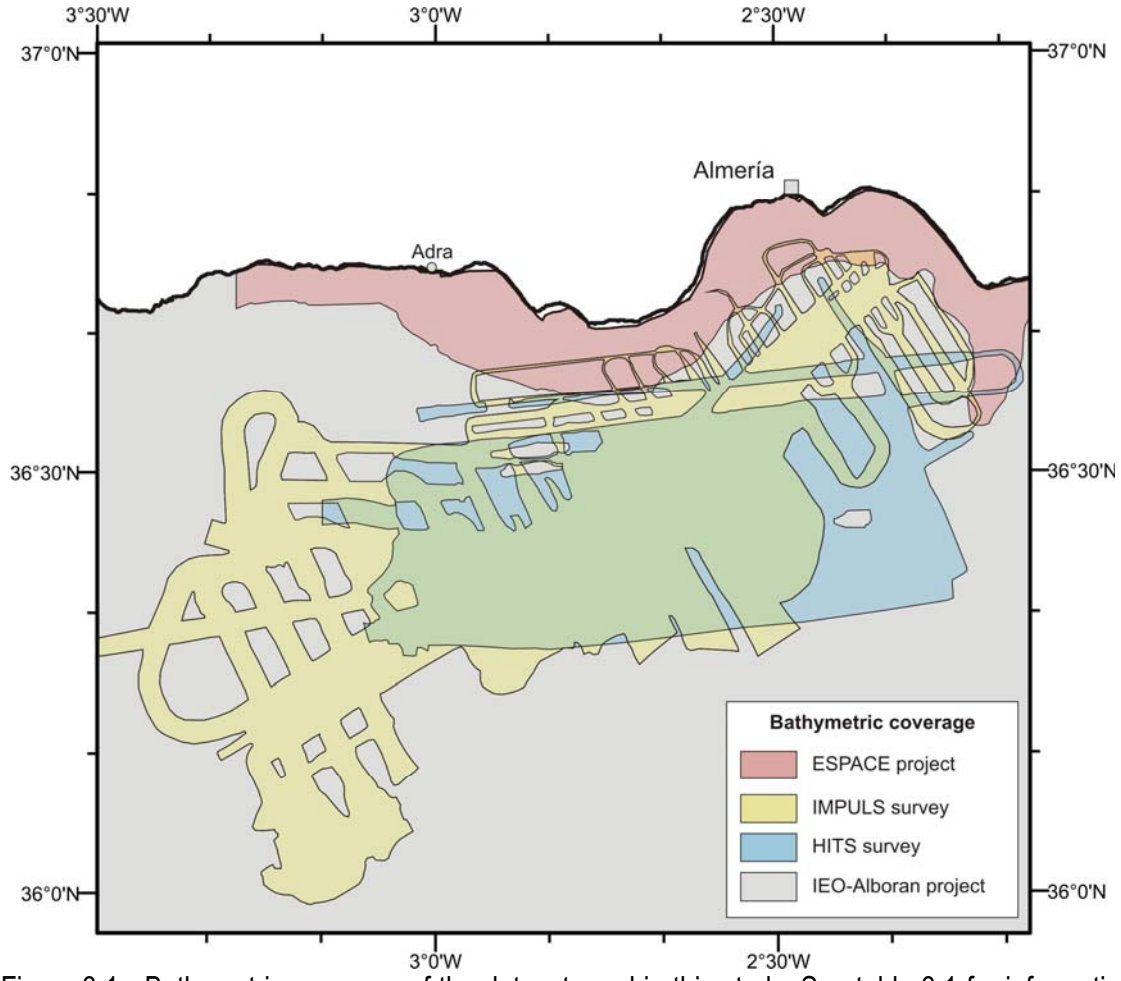

Figure 3.1. Bathymetric coverage of the dataset used in this study. See table 3.1 for information on the surveys.

All bathymetric data were compiled and processed at the Unidad de Tecnología Marina (UTM) - CSIC using the *CARAIBES v3.1* submarine mapping software developed by the *Institut français de recherche pour l'exploitation de la mer* (IFREMER), which allows the processing of data from different multibeam echo-sounders. The main steps during data processing included search of possible errors due to the variations in water column SVP and motions of the vessel (roll, pitch, yaw and heave), and invalidation of the noisy external beams. Next, data was filtered and cleaned up using different geometric methods, such as automatic filtering of sounding through field triangulation, to detect punctual errors in bathymetry volumes. A final manual

cleaning with the ping graphical editor enabled us to obtain a higher accuracy of the depth data control. After filtering, bathymetric data was interpolated at nodes of a regular-spacing grid of 30 m for the IMPULS data, and 70 m and 10 m for the IEO data. The final DTMs were incorporated to the *ArcGIS* software and used to produce contour lines, slope maps and shaded maps. The same DEMs were incorporated into the *Fledermaus* software to make a 3D exploration of the bathymetric mosaic.

Table 3.1: List of marine surveys and instrumentation that provided the dataset used in this thesis. (UTM: Unidad de Tecnología Marina, CSIC: Consejo Superior de Investigaciones Científicas, IEO: Instituto Español de Oceanografía)

Survey	Year	Research Vessel	Chief Scientist/PI and Institution	Data recovered and used in this study
ESPACE	2000	*Miki I*	J. L. Sanz (IEO)	Simrad EM3000 multibeam echo-sounder (300 kHz)
HITS	2001	*Hespérides*	E. Gràcia (UTM-CSIC)	Simrad EM12 multibeam echo-sounder (12 kHz) TOPAS PS18 sub-bottom profiler TOBI sonar mosaic
500 viviendas	2002	*Vizconde de Eza*	R. Gómez /J. Acosta (IEO)	Simrad EM300 multibeam echo-sounder (30 kHz)
Alborán-02	2002	*Vizconde de Eza*	C. Palomo (IEO) - leg1 R. Gómez (IEO) - leg2 / J. Acosta	Simrad EM300 multibeam echo-sounder (30 kHz)
ESPACE	2003	*Teresa Rosa*	J. L. Sanz (IEO)	Simrad EM3000 multibeam echo-sounder (300 kHz)
Alborán-03	2003	*Vizconde de Eza*	P. Herranz / J. Acosta (IEO)	Simrad EM300 multibeam echo-sounder (30 kHz)
IMPULS	2006	*Hespérides*	E. Gràcia (UTM-CSIC)	High-resolution multi-channel seismics (GeoEel streamer) Single-channel seismics (SIG streamer) Simrad EM120 multibeam echo-sounder (13 kHz) TOPAS PS18 sub-bottom profiler Gravity corer
CarbMed	2006	*Meteor*	C. Hübscher (Universität Hamburg)	Gravity corer
EVENT-Shelf	2008	*García del Cid*	R. Bartolomé, C. Lo Iacono / E.Gràcia (UTM-CSIC)	Sparker high-resolution single-channel seismic
EVENT-Deep	2010	*Sarmiento de Gamboa*	R. Bartolomé / E. Gràcia (UTM-CSIC)	Atlas P35 parasound sub-bottom profiler Deep-penetration multi-channel seismics (Sentinel streamer)

3.1.1.3. Teledetection (airphotos and orthophotos)

The aerial photography analysis is based on the stereoscopic examination of overlapping aerial photographs taken with slightly different angles in order to create a 3D impression of the ground surface. This is a method widely used in several disciplines to make a rapid and detailed reconnaissance of the terrain. Orthophotos are orthorectified versions of the aerial photographs in order to avoid distortion and ensure uniformity of scale. Orthophotos are georeferenced images that can be included in GIS systems and be used to measure true distances.

The first reconnaissance of the entire emerged Carboneras Fault zone was undertaken by stereopair airphotos shot in 1957 (1:33.000 scale) by the Spanish air force in collaboration with the US air force for cartographic purposes. In addition, two sets of orthophotos from the *Consejería de Medio Ambiente-Junta de Andalucía* were used in this study. 1) Colour digital orthophotos, obtained from a flight survey

conducted in 1998 and 1999 (1:60.000 scale), with a 1 m resolution (each pixel of the image corresponds to a 1 m^2 of terrain), and 2) black and white digital orthophotos, obtained from a flight survey carried out during years 2001-2002 (1:20.000 scale), with a 0.5 m resolution.

The age of aerial photographs was a key factor in this study because after the flight survey in 1957 the area became rapidly covered by greenhouses and agricultural fields, making it very difficult and sometimes impossible to identify fault scarps and geomorphological limits. Morphostructural features were initially defined by stereoscopic examination of overlapping airphotos and mapped directly on orthorectified versions: spatially corrected and georeferenced air photos and more recent digital orthophotos added to the *ArcGIS* dataset. As a result of this, the main landforms and neotectonic features were recognized. This, together with field surveys along the fault, enabled the selection of zones suitable for detailed analysis.

3.1.1.4. Micro-topography

Micro-topographic maps are DTMs built by field surveying with a total station instrument: a theodolite provided with an electronic distance-meter. Total station surveying usually generates an irregular grid of points where the horizontal position and elevation are measured by a theodolite using trigonometry from vertical and horizontal angles between the base station and the measured points and the slope distance.

Small-scale neotectonic features, such as fault scarps are usually too reduced to be accurately mapped and represented on the existing topographic maps of the area. For this reason, critical faulting features at selected paleoseismic sites were mapped through total station surveying. The theodolite employed in this study is a *Leica Total Station TPS 1700* and was used at El Hacho, Pecho de los Cristos, La Pared Alta and Cerro Blanco paleoseismic sites around La Serrata. Topographic points (XYZ) were introduced in the commercial software *Cartomap* (*ANEBA*) from which irregular grid DTMs were generated and 1 m spaced contour maps were obtained by triangulation algorithms.

3.1.1.5. Onshore-Offshore geomorphologic cartography

Mapping of Quaternary landforms and deposits of the deformation zone is the first approach to paleoseismic analysis, and it is often the most fruitful process. According to McCalpin (2009) “trenches should never be sited until the geomorphic relations in the area of investigation are thoroughly understood”. Although the field survey, which is a direct technique, plays an important role in geomorphological cartography onshore, in this work, indirect techniques such as airphotos and acoustic

backscatter models, were essential for building this cartography. Topographic and bathymetric maps constitute the base of this cartography.

As a first approach, an analysis and a fault trace cartography of the entire onshore-offshore Carboneras Fault was performed to evaluate the sites with the most evidence of recent tectonic activity. Onshore, this first observation was done using aerial photos (1:33.000 scale) and the fault trace was drawn in 1:50.000 scale topographic maps. Offshore, cartography was elaborated through high-resolution swath-bathymetry mosaics and backscatter information with a regular-spacing grid of 30 m. A second approach consisted in a more detailed cartography of the fault trace and the materials involved in the Quaternary movements of the fault, including a very detailed cartography of La Serrata, located in the central section of the emerged Carboneras Fault, and the entire Almería margin. Onshore Quaternary deposits, rock formations and morphological features with evidence of the recent evolution of the fault zone were mapped in 1:5.000 scale topographic maps through the analysis of stereopair photographs, DTMs, orthophotos and meticulous field survey along each fault trace. Offshore, the active fault traces were accurately located using seismic profiles and drawn on a regular-spacing grid of 10 m bathymetric mosaic was used for most of the fault trace. A third approach was adopted onshore through exhaustive mapping in selected paleoseismic sites using the detailed microtopographic cartography as basemap. This corresponds to the previous step before opening trenches in order to better understand the geomorphologic relationships in the field.

Geomorphical cartography of the deposits associated with the Carboneras Fault zone, both onshore and offshore, helped to determine deformed geomorphical surfaces, mass wasting deposits and other elements, such as offset channels. Fault slips could be inferred from the estimated ages of these features and their measured displacements.

3.1.2. Sub-surface analysis (stratigraphic evidence)

The analysis of the land-surface concerns a very small portion of the effects of the fault movement. To have an in-depth understanding of the fault, and to obtain long-term paleoseismic parameters, we need to survey the sub-surface structures. Sub-surface techniques allow the detection of the stratigraphic evidence of seismic activity in a given terrain, such as offset horizons, folded & faulted reflectors, shearing zones and discontinuities. For this reason, sub-surface layers of marine and terrestrial environment are imaged using indirect geophysical techniques, such as seismic reflection profiling, Ground Penetrating Radar or magnetotellurics.

3.1.2.1. Reflection seismology

Seismic reflection systems are based on the propagation of sound waves generated by a seismic source (e.g. air guns), which are partially reflected in the earth surface and subsurface boundaries with different physical properties (i.e. velocity propagation and density). The reflected wave is registered and digitalized by the receivers (e.g. geophones or hydrophones) generating seismic traces. After processing the seismic signal, seismic traces are stacked to obtain a preliminary seismic cross section that can be subsequently improved by post-stack processing. Selecting a seismic source implies a trade-off between penetration, which demands lower frequencies (e.g. airgun), and resolution, which requires greater bandwidths (e.g. Sparker, 3.5 kHz sounder, parasound, chirp). In marine seismic surveys, the source and streamer (a string of hydrophones separated at regular intervals) are towed behind the vessel just below the sea-surface, allowing a relatively fast acquisition of seismic lines. A large amount of information is acquired from a marine seismic reflection survey, which usually demands an extensive processing before obtaining a seismic cross section image that can be geologically interpreted. In scientific literature, seismic cross sections are often shown with some vertical exaggeration (exaggeration in the vertical to horizontal aspect ratio). Thus, angular relationships in stratigraphic and structural architectures are distorted and this needs to be taken into account when obtaining paleoseismic results. Vertical exaggeration is carried out in order to optimize visualization, such as placing emphasis on stratigraphic architectures or displaying long sections that would otherwise not be workable (Stewart, 2010).

To image the geometry of the offshore segment of the CFZ with different scales of resolution and penetration, four seismic systems were used during different cruises: deep penetration MCS (DP-MCS), high-resolution MCS (HR-MCS), single-channel *Sparker* and Parametric echo-sounder (TOPAS) (Fig. 3.2 and 3.3) (Bartolomé et al., 2009). Specification of sources, receivers and acquisition systems are decribed in the following sections. Moreover, seismic lines from other surveys (Fig. 3.2) were consulted in order to have a preliminary overview and to obtain velocity models.

Deep-penetration multichannel seismics

During the 2010 EVENT-Deep survey onboard the RV Sarmiento de Gamboa, one deep-penetration multichannel seisimic (DP-MCS) profile (EVE-2b) was acquired across the Carboneras Fault in order to see the internal architecture of the fault at depths not reachable by other seismic systems (Gràcia et al., 2010; Bartolomé et al., 2010). In the stacked profile, reflections as thin as 4 ms (approx. 3 m thick) can be distinguished in this line (Fig 3.3). However, at the moment of presenting this thesis, the processing of the EVE-2b profile was not finished and thus will not be presented.

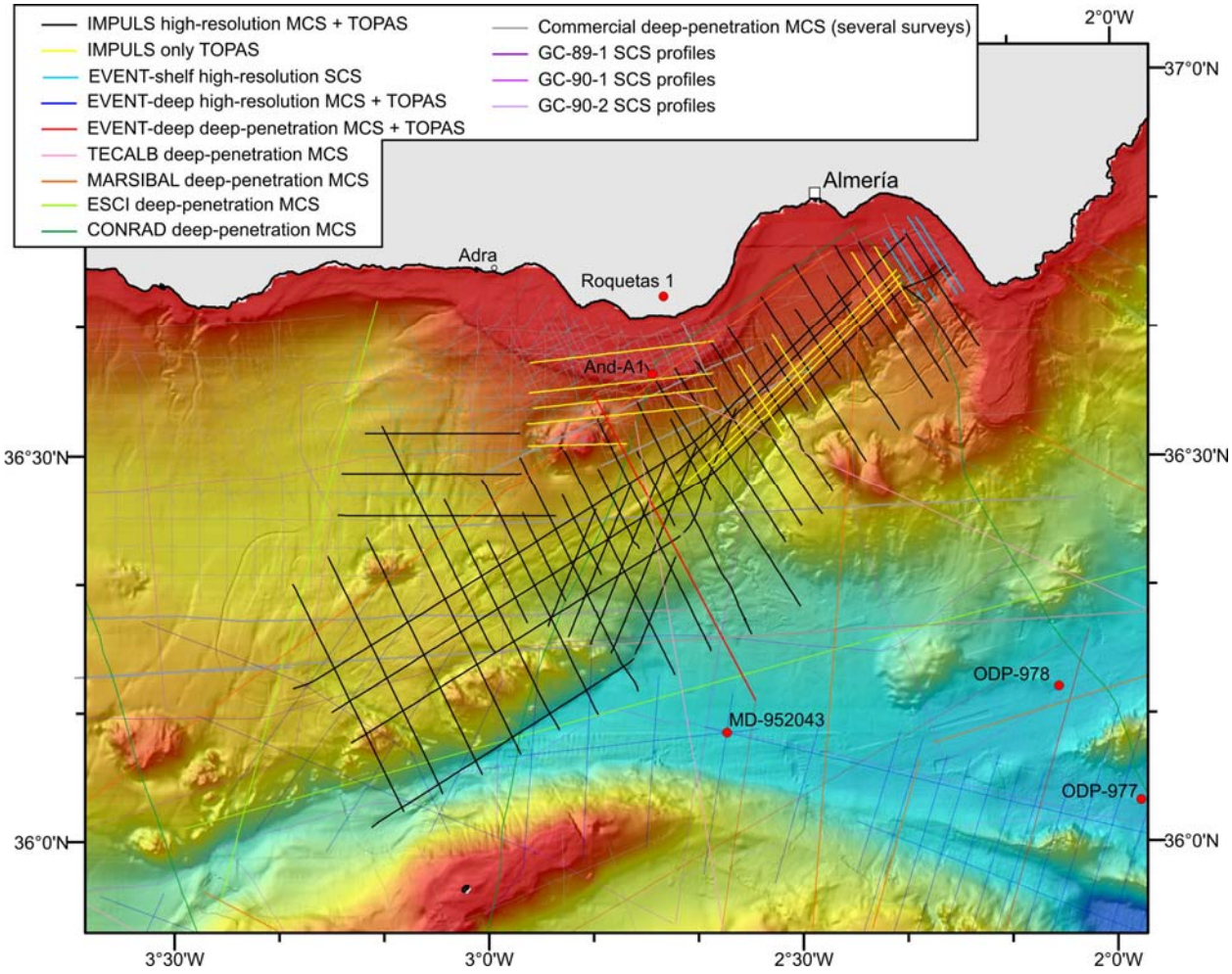

Figure 3.2. Seismic lines around the Carboneras Fault zone from diverse surveys. The seismic dataset used in this study the thick ones.

High-resolution multichannel seismics

A "GeoEel" Geometrics (USA) digital streamer was used during the 2006 IMPULS survey onboard the RV Hespérides to record high-resolution multichannel seismic (HR-MCS) data across and along the Carboneras Fault. The streamer had 300 metres of active section (6 active sections of 50 metres each) and each of the active sections was configured to form 8 channels, totalling 48 channels 6.25 m apart. The streamer was towed at 2 m depth. The seismic source used during the IMPULS survey was a 10 m long array comprising eight guns: four Bolt (model 900LLX-T) and four Sleeve Guns I. Models and simulations using the *Gundalf* software designed an adequate signal for the high resolution required, with band width reaching up to 300 Hz. During the IMPULS cruise, sampling rate was at 1 ms. Triggering was calculated to be every 10-12 s (25 m), or 5-6 s (12.5 m) depending on the water depth (Gràcia, 2006).

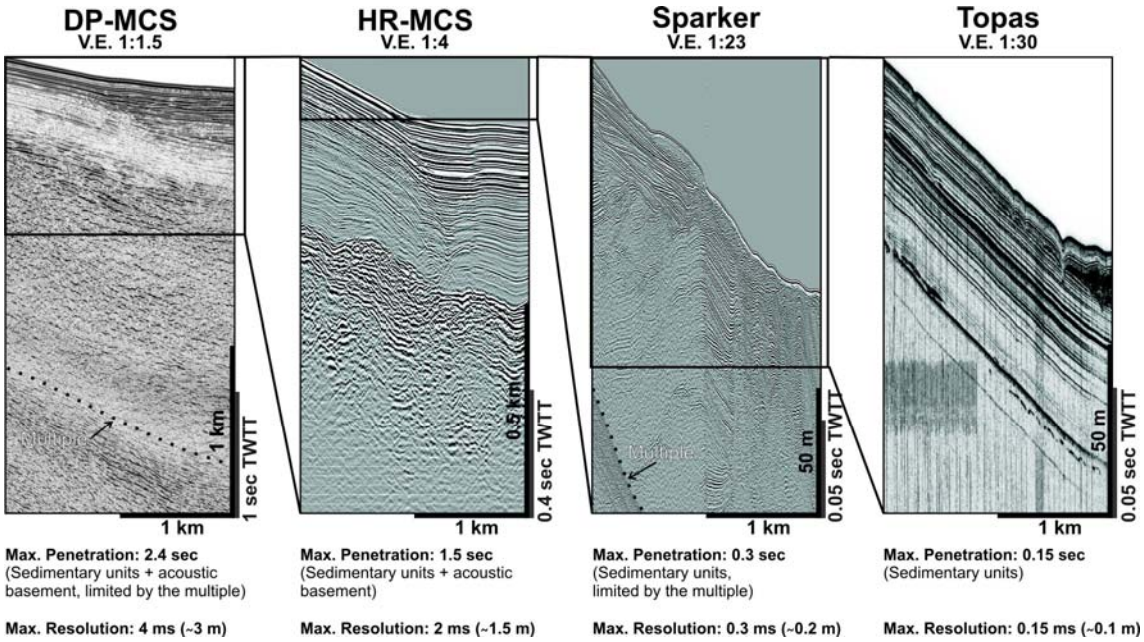

Figure 3.3. Comparison of resolution and penetration between the four seismic systems used in this study along 2 km of profile (different line sections are shown). See text for explanation. V.E.: Vertical Exaggeration.

A total of 47 profiles, corresponding to 1419.6 km of data, were processed by Dr. Rafael Bartolomé and collaborators. During the survey onboard, a basic preliminary processing sequence was imposed as a quality control test using the *Promax software*. The flow sequence started with a re-sampling from 1 to 2 ms, a static correction of 50 ms due to the existing lag between the recording window and shot triggers, and a top mute picking. Then a FK filter (using a fan filter of ±3000 m/s, between 20 and 200 Hz) was applied to reduce spatial aliasing and a bandpass filter minimum phase (20-25-170-200 Hz). A predictive deconvolution and a NMO (Normal Move Out) correction with a constant velocity of 1700 m/s due to the reduced length of the streamer were also applied to the data. Finally, a CDP (Common Depth Point) stack was executed. In a further and more detailed processing, post-stack velocity analysis was carried out using the *Promax software* at the *Laboratori de Processat* of the UTM-CSIC. Three main seismostratigraphic units where identified: Neogene basement, lower, and upper sedimentary units. The units were distinguished from geometrical relations and seismic facies of the reflectors. Analysis of velocities based on commercial seismic lines (line AG-6 from ENAPSA-1972, lines AS-38, AS-42 from WESTERN-1977 and lines AM-110, AM-112 from ELF-AQUITANE-1978) (Gessal, 2011) helped to assign the velocity range to each of the seismic facies for a *Fast Explicit* migration to better constrain the geometry. Time-migrated seismic lines were incorporated into a *Kingdom Suite* project for analysis by delineating key horizons and structures along the profiles.

The window acquisition for the IMPULS HR-MCS profile was 4 seconds, although no more than 1.5 sec of penetration was achieved with the seismic source used in this high-resolution experiment. Nevertheless, all the sedimentary seismic units, with maximum thickness of 1 sec (approx. 1 km) are clearly observed, and especially the upper units which were the main goal of this survey. Below the acoustic basement top, around 0.4 sec of disperse reflections can be observed. Reflections as thin as 2 ms (around 1.5 m thick) can be distinguished with this system (Fig 3.3).

Very high-resolution single-channel seismics: Sparker system

In summer 2008, very high-resolution single-channel seismic (SCS) data were collected during the EVENT-Shelf cruise onboard the RV Garcia del Cid. Five Sparker profiles across the CFZ on the shelf were acquired to observe the onshore-offshore link of the fault, where a shallow-water multiple prevents the acquisition of a clear MCS image. It also provided accurate morphostructure images in the sub-surface and the upper geometry of the fault. The seismic system employed was a "GEO-SPARK" source from Geo-Resources Company (Rotterdam, The Netherlands). A 6 kJ Sparker system was used and triggered every 2 s. The receiver was composed of 9 m long, 24 hydrophones single-channel streamer. The first processing of data entailed a change of polarity because the system uses a negative electric discharge pulse in order to reduce the wear of the tips. The processing sequence continued with debias, minimum bandpass filter (350-1500 Hz), AGC (10 ms window), gain constant (1-3 dB depending of the profile) and spherical divergence to recover the loss of energy. Finally, an automatic or manual "swell filter" depending on the seafloor topography was performed (Bartolomé et al., 2008).

The window acquisition for the EVENT-Deep Sparker profiles was 0.4-1 seconds, depending on the profile. In most of the profiles the sea-bottom multiple reflection prevents observation below it, and a maximum of 0.3 ms (approximately 250 m) of sedimentary seismic units under the seafloor can be observed. Reflections as thin as 0.3 ms (around 0.2 m thick) can be distinguished in the Almería shelf area with this method (Fig 3.3).

Sediment profiler TOPAS

The TOPAS (TOpographic PArametric Sonar) system is a high-resolution sub-bottom profiler with parametric effect. It uses a primary frequency of 18 kHz, and a secondary frequency of 1 to 6 kHz. The first systematic survey of the Almería Margin with TOPAS sediment profiler was carried out during the HITS-2001 cruise, mainly devoted to TOBI sidescan sonar survey with the result that the profiles were acquired parallel to the slope. The obliquity of the TOPAS profiles with the fault prevented the acquisition of a realistic image of the faulted reflections. Although these profiles are not

shown in this thesis, they provided valuable preliminary results (Gràcia et al., 2006) to guide the planning of the IMPULS survey. This survey was specifically designed to analyse the deep-structure and activity of the Carboneras Fault. During the IMPULS 2006 marine survey onboard the RV Hespérides, a *TOPAS PS18* designed by *Simrad*^{TM} was employed simultaneously with the other geophysical methods to obtain detailed stratigraphic information about the uppermost tens of metres below the seafloor across and along the Carboneras Fault. A Chirp pulse wavelet with frequencies of 1.5 – 5 kHz was used during the IMPULS cruise. The pulse length was 20 ms with a triggering rate of 1.5 seconds. A total of 60 TOPAS seismic profiles corresponding to more than 1410.66 nm were acquired during the IMPULS cruise. Most of the profiles are perpendicular to the CFZ (NW-SE) although some profiles were acquired parallel to the fault in order to investigate strike-slip displacement (Gràcia, 2006).

The window acquisition for the TOPAS IMPULS profiles was 0.4 seconds. The penetration of the sedimentary units reaches 0.1 sec (approximately 75 m) below the sea-bottom although weak reflections can be observed down to 0.15 sec (aprox. 110 m) below the sea-bottom in particular cases. Reflections as thin as 0.15 ms (around 0.1 m thick) can be distinguished using this system in the Almería Margin (Fig 3.3).

3.1.2.2. Magnetotellurics

The magnetotelluric (MT) method is a passive electromagnetic technique that consists in measuring temporal fluctuations in the natural electromagnetic field on the Earth's surface. These fluctuations obtained in the frequency domain allow us to determine and image the electrical resistivity at depth (Simpson and Bahr, 2005). Variations in the resistivity value are related to changes in rock properties such as lithology, structure, porosity and fluid content. Audiomagnetotellurics (AMT) is based on the same principles as magnetotelluric methods but uses higher frequencies obtaining a higher resolution of the upper kilometres.

In order to observe the onshore subsurface structure of the CFZ and the surrounding basins, an AMT survey was carried out by the EXES geophysics team from the *Departament de Geodinàmica i Geofísica* from the *Universitat de Barcelona*. An AMT profile was obtained across the La Serrata range in the central section of the emerged Carboneras Fault. A total of 24 AMT sites were measured with a *Stratagem* equipment from *Geometrics* and 13 MT sites were measured with an *ADU06* system from Metronix. From these measurements, only 29 were selected for building the profile. Noisy channels or other acquisition problems were discarded and only the sites with sufficient quality were used. The frequencies range between 96 kHz and 10 Hz down to 100 s. This range of frequencies showed different resistivity regions beneath La Serrata down to 2 km in a resistivity range between 4 and 750 Ω m. The maximum separation between continuous sites was 1.3 km corresponding to distant sites from the

fault zone, and the minimum was 40 m corresponding to sites closer to the fault traces within the La Serrata range.

3.1.2.3. Ground Penetrating Radar

Ground-penetrating radar (GPR) systems are based on the same principles as reflection seismology: transmitted waves that are reflected and then detected by a receiver on the surface. The main difference lies in the source, i.e. GPR works with transmitted electromagnetic radiation with frequencies from 80 to 300 MHz. As in seismic systems, the higher the frequency used, the higher the resolution obtained although less penetration is achieved. Images of the subsurface generated by GPR are similar to those of seismic profiles. Subsurface contacts with higher contrasts in dielectric properties return stronger reflections. Penetration depth is strongly dependent on a) the antenna frequency applied, b) the geophysical parameters of the material studied (permittivity and conductivity), c) the presence of water-saturated or clayey sediments, and d) the prevailing weather conditions (Reicherter and Reiss, 2001). Materials with high electrical conductivity such as clay or fluids with a large amount of dissolved solids will rapidly decrease the maximum depth of penetration.

Two GPR surveys along the Carboneras Fault were conducted with different approaches at the El Hacho site (La Serrata, central section of the emerged Carboneras Fault). The GPR work started as collaboration with the EXES geophysics team from the *Departament de Geodinàmica i Geofísica* from the *Universitat de Barcelona* with paleoseismic purposes. This collaboration developed into a PhD thesis currently being carried out by Miquel Coll, who was involved in the GPR acquisition, performed the data processing and contributed to the interpretation. The results were discussed to combine the geophysical and paleoseismic aspects. Only a small part of these results will be shown here as the whole dataset and results will form part of the thesis of M. Coll. The first survey (June 2005) was planned as a pre-trenching study, to identify the major fault traces so as to determine the most suitable location of the trenches. In addition, the acquisition served as a test survey for using the GPR techniques in such a dry environment. A *Pulse Ekko 100* system was employed using 25, 50, 100 and 200 MHz antenna sets obtaining six different profiles, across and along the fault trace. The 25 MHz antenna allowed imaging down to 10 m depth, the 50 MHz antenna around 6 m depth (depending on the material), the 100 MHz antenna down to 4.5 m depth and 200 MHz antenna down to 3 m depth. The CMP velocity profiles were obtained to convert wave travel times to depth. A total of 5 profiles were obtained in a continuous mode and one (the 25 MHz profile) in a step-by-step mode. The second survey, in January 2007, was carried out in collaboration with the geophysics team from the Institute of Neotectonics and Natural Hazards (RWTH) from Aachen University (Germany). The GPR survey was developed in parallel with a 3D trenching survey in order to complete

and extend the information obtained from the trenches. A total of 17 GPR profiles were acquired with a GSSi5104 system using a 270 MHz sheltered antenna. In both GPR surveys, topographic profiles along the GPR lines were obtained with a Total Station in order to adjust profiles to the real topography.

3.1.2.4. Electrical Resistivity Tomography

Electrical resistivity tomography (ERT) is a technique for measuring and imaging the apparent subsurface resistivity of the ground using conduction currents. From a series of electrodes, low frequency electrical current is injected into the subsurface, and the resulting potential distribution is measured (Lytle and Dines, 1978). Real resistivity models are obtained by inversion processes of the measured potential distribution. The result is a pseudo-section that distinguishes between bodies of the subsurface with different values of resistivity.

In parallel with the 2005 GPR survey and with the same aims, a 2D ERT survey was undertaken to combine both systems. The ERT survey was also conducted in collaboration with the *Departament de Geodinàmica i Geofísica* from the *Universitat de Barcelona*. The tomography array used at the El Hacho site is a *GEOFYZIKA* system with a Wenner-Schlumberger distribution of 24 electrodes 2 meters apart. Two ERT pseudo-sections were acquired reaching down to a depth of 5 meters.

3.2. Direct techniques

3.2.1. Trenching

Trenches are long and narrow ditches used in onshore paleoseismology to obtain paleoearthquake evidence and to calculate paleoseismic parameters (i.e. recurrence interval between earthquakes, elapsed time since the last earthquake, fault slip rates and fault slip per event) from stratigraphic observations (Sieh, 1978). Trenches are dug mainly across the fault to see vertical sections of the fault trace or fault zone, but trenches can also be dug along the fault trace to observe horizontal displacements of linear elements crossing the fault. The selection of the emplacement of a trench is critical for obtaining successful results. Trench sites must have easy access so that an excavator can be brought in although hand-excavated trenches can be dug at remote sites. The trench sites must be covered by the younger deposits affected by the fault. The balance between erosion and sedimentation must also be favourable. Excessive sedimentation will expose only the very young materials in the trench so that information about previous events will be inaccessible. Excessive erosion could remove all traces of paleoearthquake evidence. Thus, for an optimum selection of the trenching site, a good geomorphic understanding of the area is of paramount importance. There are different ways to work with trenches depending on field conditions (i.e. single slot to several benched trenches, manual logging versus photomosaic logging, etc) and on the geologist's preferences Trench walls should be as straight and as vertical as possible in order to obtain a well-oriented geologic section where structures, stratigraphy and soil horizons can be easily observed. However, trench walls may become unstable and unsafe because of the nature of the deposits and the humidity. This determines the maximum depth of the ditch, and whether or not to pumps to reduce the groundwater level should be used.

A total of 17 trenches were opened and 31 trench walls were logged during 3 trenching surveys in December 2005, January 2007 and January 2008 along the southwestern boundary of La Serrata. Dry conditions enabled us to dig a maximum of 3 m deep trenches with solid walls, but also a 5 m high anthropic wall was cleaned and used as a trench wall. Trenches had different lengths depending on the geomorphical conditions and on the aim, varying from 2 to 70 m, although in most cases trenches were around 20-30 m long. The methodology used for trenching in this study is described below. After digging the trench, the walls were cleaned with scrapers and brushes so as to remove the soil smeared on the walls during excavation. Then, a reference grid for logging was constructed with horizontal lines of nylon string, usually spaced 1 m apart and attached to the trench wall by large nails. A photo was shot of each cell and all photos were retro-deformed in order to adjust them to an established scale. Photos were placed together to obtain an undeformed photo-mosaic corresponding to a real image of the trench wall. The photo-mosaic was used to log the

stratigraphic, pedogenic and tectonic limits while observing the trench wall, but also served as a graphic record. Geological contacts identified in the trench wall were highlighted by placing nails with coloured flags along the contact. These contacts were drawn in the log together with textural features and indications, such as dating samples extracted from the trench wall. Finally, the log was digitized to obtain a vectorial drawing to reflect the interpretation of the paleoearthquake history from the trench wall analysis.

3.2.2. Marine sediment cores

Ground-truthing and seafloor sampling is necessary to characterize and date the marine deposits. Gravity corers are one of the simplest ways of obtaining sediment cores from the seafloor. A corer consists of a barrel, a cutter at the nose, and a weight at the top end with a valve to allow expulsion of water. Gravity cores are lowered from a vessel on a wire to the seabed. A simple "catcher" at the nose cone prevents the sample from sliding back out of the core tube (Goldfinger, 2009).

In order to complete the necessary information for the paleoseismic and neotectonic study of the CFZ offshore, 6 gravity cores (Table 3.2) were acquired near the fault zone. In spring 2006, during the IMPULS survey onboard the BIO Hesperides, four gravity cores (CIM-1 to CIM-4) were acquired at selected sites with high-resolution imaging. However, because of poor sea conditions, two of the sediment cores were obtained some km from the target sampling sites. Some months later, during the CARBMED cruise onboard the RV Meteor, coring at the two selected stations was successfully undertaken (M69/1-340 and -349) and a third additional core was acquired (M69/1-348). The main aim of sediment coring was to characterize possible paleoearthquake deposits (e.g. turbidites) on the basis of their texture, physical properties and geochemical analyses, and to obtain the age of these sediments. Sedimentation rates were obtained to estimate the ages of key reflections observed in high-resolution TOPAS profiles. Moreover, a paleoclimate study based on these cores is currently being undertaken out by Dr. Graziella Bozzano (previously at the ICM-CSIC and now at the Servicio de Hidrografía Naval of Buenos Aires, Argentina).

During both surveys, sediment cores were stored in cold conditions awaiting laboratory analyses. Once opened, the sedimentological characteristics were described in both half-sections (i.e. colour, structures, lithology, facies), physical signatures were measured in the archive half-section, and geochemical parameters were analyzed from samples taken from the working half-section. This information allowed us to establish the stratigraphic fingerprint of the marine sediments. The sediment texture (i.e. grain-size) of CIM and M69 cores was measured at the *Institut de Ciències del Mar* (ICM)-CSIC using a large-diameter settling tube for the coarse-grained fraction (>50 μm) and a *Sedigraph III* (model 5000D) from *Mocrometrics* for the fine-grained fraction (<50

μm). Sediment physical properties (magnetic susceptibility, gamma ray from which density is derived, and P-wave velocity) were measured at ICM-CSIC laboratories (CIM cores) and at Bremen University (M69 cores) using the *GEOTEK* multi-sensor core-logger. Colour spectrophotometry, from which lightness (L*) and colour parameters a* and b* are obtained, was performed with a *Minolta 2600d* hand-held spectrophotometer in all cores. Measurements of geochemical elements were obtained for M69 cores using an X-ray fluorescence (XRF) core scanner at the University of Bremen, Germany. The total carbonate content of both CIM and M69 cores was determined from discrete samples at the ICM-CSIC sedimentology laboratory. In addition, a robust biostratigraphy planktonic foraminifera study was performed by Dr. Alessandra Asioli from the *Istituto Geoscienze e Georisorse - Sezione di Padova* from the Italian National Research Council (CNR). Selected planktonic foraminifera samples were sent to NOSAMS for Radiocarbon dating.

Table 3.2: List of the gravity cores obtained during the IMPULS and Carbmed surveys in 2006 and used for this study. MS: magnetic susceptibility, D: density, PW: P-waves, por: porosity, imp: impedance, L*: lightness, b*: , Carb: carbonate, GS: grainsize

Survey	Core name	Core length (cm)	Latitude	Longitude	Water depth (m)	Number of ^{14}C samples	Other measurements
IMPULS	CIM-1	415	36º 37.93' N	2º 30.34' W	350	5	MST: MS, D, PW Grainsize, L*, Carbonate
IMPULS	CIM-2	174	36º 36.43' N	2º 32.38' W	406	0	MST: MS, D, PW Grainsize, L*, b*, Carbonate
IMPULS	CIM-3	192	36º 27.44' N	2º 44.48' W	862	7	MST: MS, D, PW Grainsize, L*, b*, Carbonate
Carbmed	M69/1-340 (analogous to CIM-3)	327	36º27.55' N	2º 43.59' W	868	8	Grainsize, L*, Carbonate MST: MS, D, PW, por., imp. XRF: Fe, Ca, Al, K, Ti
Carbmed	M69/1-348	557	36º27.43' N	2º 48.63' W	802	11	L*, Carb., GS, MST: MS, D, PW, por., imp. XRF: Fe, Ca, Al, K, Ti
Carbmed	M69/1-349 (analogous to CIM-2)	215	36º36.62' N	2º 31.74' W	395	5	L*, Carb., GS, MST: MS, D, PW, por., imp. XRF: Fe, Ca, Al, K, Ti

3.2.3. Radiometric dating methods

In order to investigate the paleoseismic history of a structure or region, it is essential to know the age of the Quaternary deposits involved in the deformation. This is why radiometric dating methods are widely used in Paleoseismology. Radiometric dating is based on a comparison between the observed abundance of a naturally occurring radioactive isotope and its decay products, using known decayment rates.

Dating in paleoseismic studies constrains the age of the deposits in order to bracket the timing of recent fault movements. These ages will allow us to calculate paleoseismic parameters, such as the recurrence interval, the elapsed time since the last earthquake and slip-rates. Nevertheless, to interpret a radiometric age a good background of the geological and pedogenic history of the dated material is

indispensable. It is also essential to understand the nature of the deposit and the processes that occurred during the evolution of this material. An analysis of only one sample yields little information. Ideally, independent methods should be used to date a deposit, and only if results are internally consistent and fit in with the geological context, should they be considered as a reliable.

Four different techniques were applied in this study depending on the nature of the material and the estimated age. Radiocarbon (mainly accelerator mass spectrometry (AMS) ^{14}C) was used to date Holocene and Late Glacial sediments both onshore and offshore. Uranium series (U/Th), Thermoluniscence (TL) and ^{10}Be cosmonuclides isotopes were used for older onshore deposits.

3.2.3.1. Radiocarbon (^{14}C)

The radiocarbon dating method uses the radioisotope ^{14}C naturally formed by cosmic rays in the atmosphere to estimate the time lapse since the death of a living organism. Plants fix atmospheric CO_2 into their organic structure through photosynthesis, incorporating the present atmospheric proportion of $^{14}C/^{12}C$. Organisms consuming plants will contain the same radio-isotopic ratio. After the death of plants or organisms, the ingestion of ^{14}C ceases and this radioisotope will start to decay at a fixed exponential rate, diminishing the $^{14}C/^{12}C$ ratio. Comparison of the remaining ^{14}C fraction of a sample with that expected from atmospheric ^{14}C yields an age provided that the sample is younger than 62.000 years (Libby, 1955), although radiocarbon ages older than 35.000-40.000 are considered as having a very high uncertainty. Furthermore, radiocarbon ages present an associated error derived from the established assumption that the $^{14}C/^{12}C$ ratio has been constant in the atmosphere through time. To correct this, calibration curves formed by comparing dating results with other independent dating methods, such as dendrochronology, are used. The corrected age is referred to as calendar age. Moreover, marine radiocarbon ages have the additional complexity of the reservoir correction (ΔR) caused by 1) the delay in exchange rates between atmospheric CO_2 and ocean bicarbonate, and 2) the dilution effect due to the mixing of surface waters with the upwelling of old deep waters. This could give rise to differences of 400 radiocarbon years between terrestrial samples and marine shells (Stuiver and Braziunas, 1993). A reservoir correction must therefore be applied to any conventional marine date. Reservoir corrections for the world oceans are obtained from paired shell/wood dates that yield an apparent age of the water in which the marine animal lived, and these dates are compared with those of stratigraphically correlated terrestrial material (e.g. Monge Soares and Alveirinho Dias, 2006). The published marine reservoir corrected values may change between localities and through time (i.e. Kovanen and Easterbrook, 2002) but they are used as a better approximation than uncorrected values.

Onshore, radiocarbon was used when possible, but sedimentary units were often beyond the limits of the dating method. The preferred radiocarbon samples in the trenches were charcoal although snail shells were also analysed. Samples were taken from the loose sediments with metallic forceps and spatula and placed into a glass jar, taking care to avoid plastic organic contamination. Samples were weighted in a precision balance and key samples with enough weight were sent to *Beta analytics Inc. laboratory* (Florida, USA) and to the *National Ocean Sciences AMS (NOSAMS)* facility (Massachusetts, USA). A total of 14 samples obtained from trench walls and natural outcrops were dated by Radiocarbon, 10 of them by Accelerator Mass Spectrometry (AMS) ^{14}C because of the small amount of sample available. ^{14}C ages measured by the laboratory were calibrated to calendar ages with the Calib 5.0.2 calibration software (Stuiver and Reimer, 1993) using the INTCAL-04 curve (Reimer et al., 2004), which calibrates ages down to 26.000 Cal yr BP. For the few samples with radiocarbon ages older than 26.000 years the Fairbanks curve (Fairbanks et al., 2005), extending down to 50.000 cal years BP, was used.

Offshore, a total of 34 hemipelagic sediment samples recovered from six gravity cores were selected for radiocarbon dating. Between 7 and 10 mg individual foraminifera (calcareous microfossils) preferably from the same species and with a diameter larger than 250 μm were hand-picked. Foraminifera were prepared and dated at the National Ocean Sciences Accelerator Mass Spectrometry Facility (NOSAMS-WHOI laboratory, Woods Hole, USA). For marine samples, the reservoir age used in this study is taken from the Malaga station (reference 217): $\Delta R = 22+/-35$ (Stuiver and Braziunas, 1993; Stuiver et al., 2005). With the local ΔR, the measured ^{14}C laboratory date was calibrated using the MARINE-04 calibration curve (Hughen et al., 2004) included in the OxCal 4.0 software (Ramsey, 2008) or Calib 5.0 (Stuiver et al., 2005) calibration softwares.

3.2.3.2. Uranium-series disequilibrium method (U/Th)

The U/Th dating technique is based on the natural disintegration of ^{234}U (present in rocks and sediments) to produce ^{230}Th. The high solubility of Uranium facilitates its incorporation into underground waters, transportation and subsequent precipitation. Thus, ^{234}U will be incorporated within sedimentary deposits or cracks in the new carbonate-rich deposit. Ideally, soon after precipitation, the new carbonic material will have a stable uranium concentration and an insignificant amount of Thorium. From that point, the ^{234}U starts its disintegration, forming ^{230}Th. Nominal dates are calculated from the daughter/parent ratio ($^{230}Th/^{234}U$) assuming that all the ^{230}Th was formed by *in situ* decay from contained ^{234}U, with dating ranges between 5 ka and 350 ka with an optimum dating range falling between 20 and 200 ka (Ku et al., 1979; Radtke et al., 1988). Nevertheless, a typical problem associated with this dating method arises when

detritric particles (such as clays) are mixed within the new carbonic material. Detritric particles are usually enriched in both elements contributing U and Th radioisotopes in an unpredictable manner. Isotopic results may provide evidence of this contamination by comparing the $^{230}Th/^{232}Th$ ratio. After Díaz-Hernández and Julià (2006) when this ratio is below 10, the age may be assumed to be contaminated producing an overestimation of the age of the sample. The Isochron technique (Bischoff and Fitzpatrick, 1991) consisting in the independent analysis of three samples may be applied to remove detrital contamination. The results are plotted and the isochron curve is obtained where the amount of contamination can be estimated.

In Southeast Spain, calcrete crusts are commonly found on top of Pleistocene alluvial fans. A total of 17 calcrete crust samples were collected arround La Serrata to for dating by the U/Th method. Selected samples present laminar facies and were carefully separated in order to avoid clastic material contamination. Samples were analysed at the *Instituto de Ciencias de la Tierra Jaume Almera-CSIC* where the Total Sample Dissolution technique (Bischoff and Fitzpatrick, 1991) was applied in order to overcome the evident clay impurity. The isotopic composition was determined by alpha spectroscopy following procedures described in Bischoff et al (1988), and the Isochron technique was applied whenever possible.

3.2.3.3. Thermoluminiscence (TL)

TL dating is based on the fact that all buried materials are exposed to a constant flux of ionising radiation from cosmic radiation and from radioactivity produced by deposits. When crystalline materials are exposed to ionising radiation, a redistribution of electrical charge occurs within the crystal, and a small fraction of the displaced charge can become trapped for long periods in higher energy states. The extra energy that the crystal contains as a result of radiation exposure can be released by heating the material. When heat is applied, some of the released energy appears in the form of light, causing the material to luminesce. This effect is known as thermoluminescence and it appears only while irradiated crystals undergo a progressive temperature increase. TL date measurement consists of two distinct measurements. The first measurement involves TL examination of the sample, and results in an evaluation of the quantity of natural radiation to which it has been exposed. The second measurement entails estimation of the radiation levels in and around the sample, after which an assessment is made of the rate at which the radiation dose was received. By combining these two measurements, the length of time during which the sample has been exposed to radiation can be calculated (Quaternary-TL-Surveys, Web Page 2010).

Luminiscence methods are commonly used for determining the age of paleoearthquakes and for neotectonic studies (Fattahi, 2009). Thermoluminiscence was used in this study to date the deposition of fine alluvial sediments with evidence of

transport prior to deposition, which ensures exposure to daylight and the bleaching of the TL signal in the sediments. In this study 30 samples were acquired and analysed at the *Quaternary TL Surveys laboratory in Nottingham* (UK). Samples were mainly collected from artificially dug trench walls at 3 sites but also from road and quarry outcrops. In each location, the gamma dose-rate was measured. To this end, a thin hole of more than 0,6 m depth was drilled from the wall of the trench or the outcrop. A sample of the burial deposit was also collected for analysis of its radioactivity, and for assessing the water content of the sediment. In the laboratory, natural and residual (bleached sample aliquot) TL intensities, as well as TL intensity from artificially irradiated samples were calculated. Subsequently, the equivalent dose or paleodose (total dose of ionising radiation received by the sediment grains from the time of their deposition to the present day) was obtained and the ages were calculated.

3.2.3.4. Terrestrial cosmogenic nuclides: ^{10}Be

Terrestrial cosmogenic nuclides (e.g. ^{10}Be) are formed by the impact of cosmic radiation on atom nuclei forming the minerals (e.g. quartz) present at and near the surface of the lithosphere. The concentration of cosmogenic nuclides found on landforms depends on the time of exposure to cosmic radiation since its formation and on the amount of cosmonuclides lost by erosion. As a result of numerical modelling, it is possible to deduce both an exposure age and an erosion rate from a series of samples taken along a depth profile.

In order to date an Early Pleistocene alluvial fan at the foot of the La Serrata range two small anthropic outcrops, spaced 240 meters apart, were selected for depth profile sampling. In each profile, six samples were collected and processed at the *Laboratori d'Isòtops Cosmogènics Terrestres* of the Universitat de Barcelona. The dating results were recently published by Rodés et al (2011).

Sample processing implied crushing and sieving of the quartz pebbles, separation of the magnetic components and removal of the carbonate content by HCl digestions. Remaining quartz grains were cleaned using sequential HF dissolutions to remove any potential atmospheric ^{10}Be. Clean quartz cores were then completely dissolved in HF and spiked with ^{9}Be carrier. Finally, beryllium was separated by successive solvent extractions and alkaline precipitations (Bourlès, 1988; Brown et al., 1992). ^{10}Be concentrations were measured by Accelerator Mass Spectrometry at the ASTER AMS facility at CEREGE (Aix-en-Provence, France). All ^{10}Be concentrations were normalized to ^{10}Be/^{9}Be SRM 4325 NIST reference material with an assigned value of (2.79±0.03)•10-11 (Nishiizumi et al., 2007). To estimate the age of the landform and the erosion rates in both outcrops, ^{10}Be concentration data was adjusted to a numerical depth profile model by using a chi-square inverse approach (Rodés et al., 2011). Moreover, in order to control ^{10}Be inheritance of quartz pebble exposure prior to

transportation, a deep sample was collected from a quarry in the Pliocene conglomerates close to the apex of the alluvial fan (1 km far from the sample profiles).